AD-A245 632

# NAVAL POSTGRADUATE SCHOOL
## Monterey, California

DTIC
ELECTE
FEB 0 4 1992
S
B
D
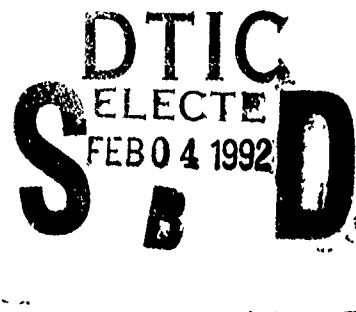
# THESIS

UNDERWATER SOUND RADIATION
FROM
LARGE RAINDROPS

by

Peter W. Jacobus

September, 1991

| Thesis Advisor: | H. Medwin |
| Co-Advisor | J.A. Nystuen |

92-02626

## REPORT DOCUMENTATION PAGE

| | |
|---|---|
| 1a Report Security Classification Unclassified | 1b Restrictive Markings |
| 2a Security Classification Authority | 3 Distribution Availability of Report |
| 2b Declassification Downgrading Schedule | Approved for public release; distribution is unlimited. |

| 4 Performing Organization Report Number(s) | | 5 Monitoring Organization Report Number(s) |
|---|---|---|
| 6a Name of Performing Organization<br>Naval Postgraduate School | 6b Office Symbol<br>(if applicable) 33 | 7a Name of Monitoring Organization<br>Naval Postgraduate School |
| 6c Address (city, state, and ZIP code)<br>Monterey, CA 93943-5000 | | 7b Address (city, state, and ZIP code)<br>Monterey, CA 93943-5000 |
| 8a Name of Funding Sponsoring Organization | 8b Office Symbol<br>(if applicable) | 9 Procurement Instrument Identification Number |
| 8c Address (city, state, and ZIP code) | | 10 Source of Funding Numbers |

| Program Element No | Project No | Task No | Work Unit Accession No |
|---|---|---|---|
| | | | |

**11 Title** (Include security classification) UNDERWATER SOUND RADIATION FROM LARGE RAINDROPS

**12 Personal Author(s)** Peter W. Jacobus

| 13a Type of Report<br>Master's Thesis | 13b Time Covered<br>From    To | 14 Date of Report (year, month, day)<br>September 1991 | 15 Page Count<br>86 |
|---|---|---|---|

16 Supplementary Notation The views expressed in this thesis are those of the author and do not reflect the official policy or position of the Department of Defense or the U.S. Government.

| 17 Cosati Codes | | | 18 Subject Terms (continue on reverse if necessary and identify by block number) |
|---|---|---|---|
| Field | Group | Subgroup | raindrops, ambient noise, acoustic radiation from bubbles |
| | | | |
| | | | |

19 Abstract (continue on reverse if necessary and identify by block number) The principal underwater sound energy radiated by terminal velocity raindrops at sea is due to micro-bubble entrainment and oscillations which occur for drops of the two diameter ranges 0.8 to 1.1 mm (Type I) and 2.2 to 4.6 mm (Type II). In the absence of bubbles, particularly between 1.1 and 2.2 mm, the impact sound radiation is significant. The Type I bubbles radiate at frequencies close to 15 kHz, whereas Type II bubbles radiate between 2 and 10 kHz, depending on the drop diameter. Therefore Type II bubbles, which are common in moderate to heavy rainfall, offer the opportunity to determine rainfall drop distribution and total rainfall rate by remote underwater listening. Type II bubbles radiate more energy when the drop and surface temperatures differ, e.g., almost twice as much energy when the drop and surface temperatures differ by 10 ° C. Type II bubbles radiate less energy in saline water, e.g., 45 % as much energy at a salinity of 35 ppt as for fresh water. The distinctive sound spectral shape for a particular diameter raindrop does not change appreciably with extreme differences of temperature (0 to 22° C ) or salinity (0 to 35 ppt). It is possible, therefore, to condense the data acquired from hundreds of drops in our laboratory into a single relation which gives the average energy radiated by a Type II raindrop as a function of drop volume, temperature and salinity. Using this relation, we find good agreement between measurements at sea and the predicted sound spectrum for an assumed reasonable drop size distribution. Also, the total rainfall rate and drop size distribution has been calculated from sound spectra measured at sea (the inverse problem.) These early successes lay the groundwork for real time measurements of total rainfall rate and drop size distributions in moderate to heavy rainfalls inferred by remote underwater listening.

| 20 Distribution Availability of Abstract<br>☒ unclassified unlimited ☐ same as report ☐ DTIC users | 21 Abstract Security Classification<br>Unclassified | |
|---|---|---|
| 22a Name of Responsible Individual<br>H. Medwin | 22b Telephone (include Area code)<br>(408) 646-2385 | 22c Office Symbol<br>PH Md |

Underwater Sound Radiation
From Large Raindrops

by

Peter W. Jacobus
Lieutenant, United States Navy
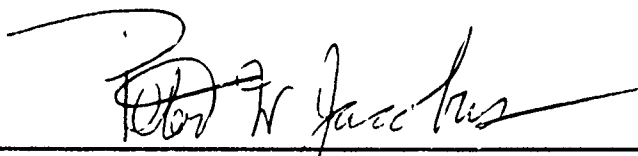B.S., University of Southern California, 1985

Submitted in partial fulfillment of the
requirements for the degree of

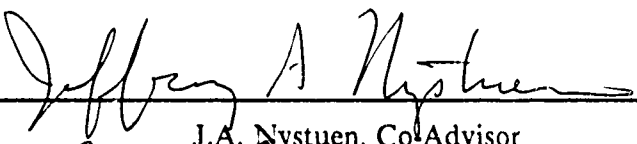MASTER OF SCIENCE IN ENGINEERING ACOUSTICS
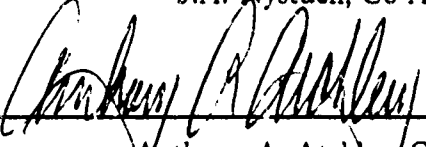
from the

NAVAL POSTGRADUATE SCHOOL
September 1991

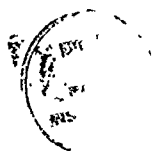Author: _____
Peter W. Jacobus

Approved by: _____
H. Medwin, Thesis Advisor

_____
J.A. Nystuen, Co-Advisor

_____
Anthony A. Atchley, Chairman,
Engineering Acoustics Academic Committee

# ABSTRACT

The principal underwater sound energy radiated by terminal velocity raindrops at sea is due to micro-bubble entrainment and oscillations which occur for drops of the two diameter ranges 0.8 to 1.1 mm (Type I) and 2.2 to 4.6 mm (Type II). In the absence of bubbles, particularly between 1.1 and 2.2 mm, the impact sound radiation is significant. The Type I bubbles radiate at frequencies close to 15 kHz, whereas Type II bubbles radiate between 2 and 10 kHz, depending on the drop diameter. Therefore Type II bubbles, which are common in moderate to heavy rainfall, offer the opportunity to determine rainfall drop distribution and total rainfall rate by remote underwater listening. Type II bubbles radiate more energy when the drop and surface temperatures differ, e.g., almost twice as much energy when the drop and surface temperatures differ by 10 ° C. Type II bubbles radiate less energy in saline water, e.g., 45 % as much energy at a salinity of 35 ppt as for fresh water. The distinctive sound spectral shape for a particular diameter raindrop does not change appreciably with extreme differences of temperature (0 to 22° C ) or salinity (0 to 35 ppt). It is possible, therefore, to condense the data acquired from hundreds of drops in our laboratory into a single relation which gives the average energy radiated by a Type II raindrop as a function of drop volume, temperature and salinity. Using this relation, we find good agreement between measurements at sea and the predicted sound spectrum for an assumed reasonable drop size distribution. Also, the total rainfall rate and drop size distribution has been calculated from sound spectra measured at sea (the inverse problem.) These early successes lay the groundwork for real time measurements of total rainfall rate and drop size distributions in moderate to heavy rainfalls inferred by remote underwater listening.

# TABLE OF CONTENTS

# LIST OF TABLES

# LIST OF FIGURES

# ACKNOWLEDGEMENTS

# I. INTRODUCTION

The oceans comprise over 70 % of the Earth's surface. Yet, although meteorologists know a great deal about the characteristics of rainfall on land, very little is known about the characteristics of rainfall at sea. Many techniques have been used in recent years, with varying degrees of success, in an attempt to estimate both the rainfall rate (and drop size distribution) over the open seas. Direct measurement by rain gages on floatable platforms are expensive and particularly difficult in heavy sea conditions. Indirect measurements such as radar and satellite imagery lack independent verification of drop size distribution. Clearly, other methods must be developed to overcome these obstacles.

Since Knudsen first measured underwater ambient sound in 1948, precipitation has been known to contribute significantly to the overall sea noise spectra. Wenz (1962) confirmed these measurements and presented a discussion of the possible noise sources. His results, shown in Figure 1 on page 2, show that wind and precipitation noise are the primary contributors of noise from 1 kHz to 50 kHz. It had been hoped that precipitation noise could be separated from wind noise, as their respective spectra have different shapes (Lemon and Farmer, 1984), and that a direct correlation between sea noise and rainfall rate would occur for this frequency band. However, early attempts to secure these results have been only marginally successful (Scrimger,et al., 1989; Tan, 1990).
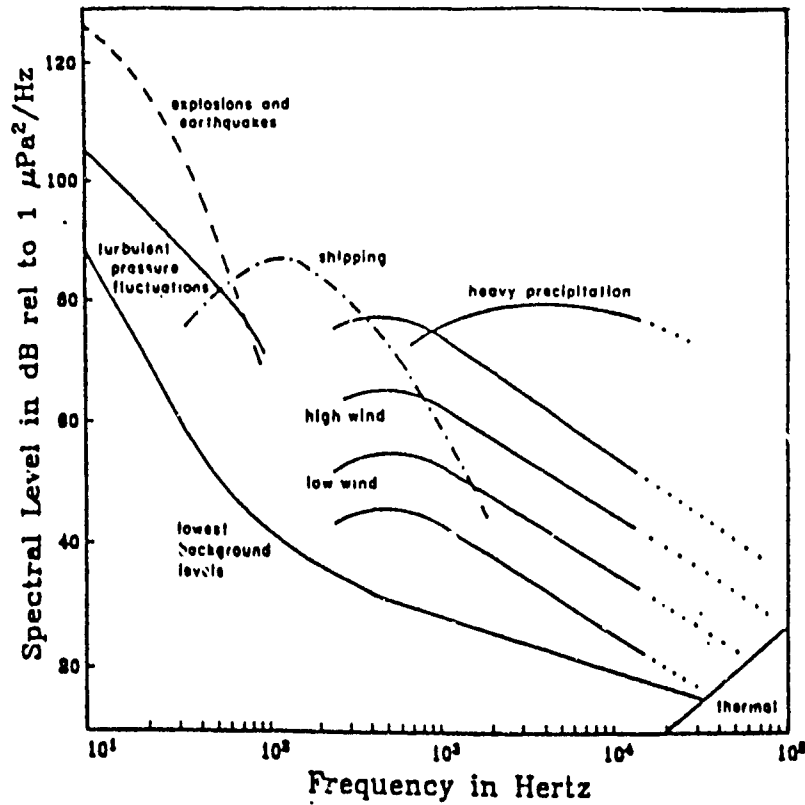
**Figure 1.** Ambient Noise Sources in the Ocean (Wenz, 1962)

Franz (1959) identified two sources of sound from an individual raindrop: the impact of the drop on the water surface, and a bubble, which is sometimes formed after a delay of at least 30 msec. This sequence is shown in Figure 2 for a 4.2 mm diameter raindrop. The bubble (when it occurs) radiates strongly with a frequency given by (Minnaert, 1933):

$$f_o = \frac{1}{2\pi a_o} \sqrt{\frac{3\gamma p_o}{\rho_\gamma}} \tag{1}$$

where $p_o$ and $\rho_o$ are the local pressure and density, $a_o$ is the equilibrium bubble radius and $\gamma$ is the ratio of specific heats ($c_p$ and $c_v$) for air, and is generally assumed to be 1.4.

2
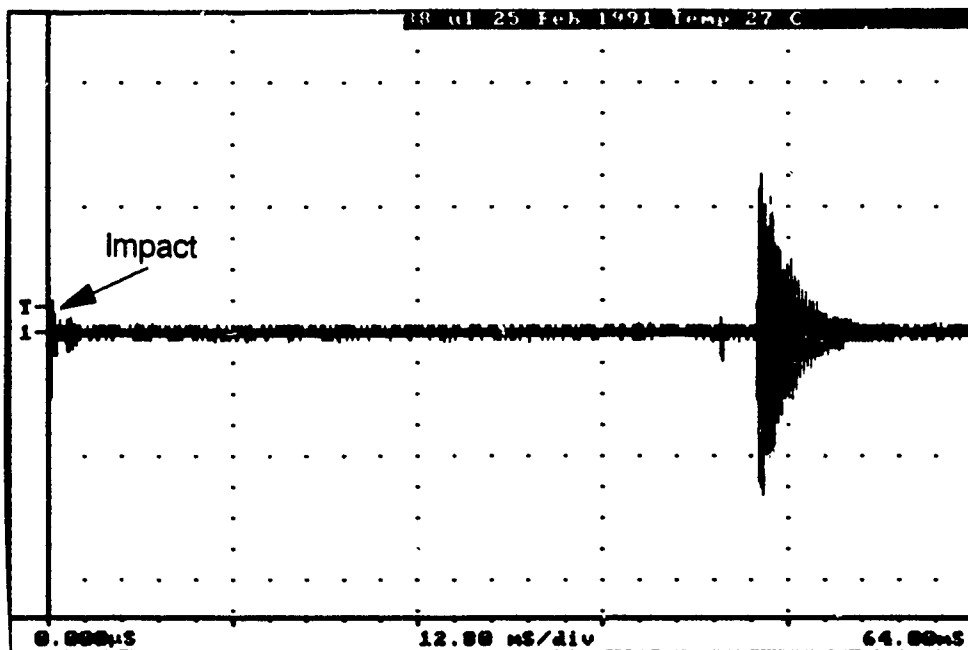
**Figure 2.** Typical Impact Followed by a Time-delayed Bubble Drop Diameter 4.2 mm; Sampling Frequency 250 kHz

Recent studies (Kurgan, 1989; Pumphrey, et al., 1989; Medwin, et al., 1990) have been centered around small raindrops ranging in size from 0.8 to 1.1 mm diameter. This diameter of drop will produce a bubble 100% of the time when falling from terminal velocity and impacting at normal incidence on a smooth surface. Since a bubble is known to radiate several orders of magnitude more energy than the impact, this might have been an important region for correlating the rainfall rate with the sound produced. Unfortunately, several separate phenomena tend to deteriorate the correlation.

Wind, which is almost always present at sea, imparts a horizontal velocity to the small raindrops. This tends to make the drops impact the surface at an oblique angle. Studies have shown that the percentage of bubble creation from small (0.8 - 1.1 mm) raindrops decreases with increasing angle of incidence: decreasing from 100% at normal incidence to 0% at about 25° (Kurgan, 1989). Also, there are other sources of bubble noise in the same frequency range of the small bubbles, such as bubbles produced by

3

breaking waves. In short, these effects make it difficult to predict rainfall rate from the sound produced by small drops.

Total rainfall rate (TRR) in mm/hr is determined by the drop size distribution, the terminal velocity and the diameter of the drops falling (Nystuen and Farmer, 1989):

$$\text{TRR} = \int_0^\infty \frac{\pi}{6} D^3 \text{n(D)} \, V_T(D) \, dD \tag{2}$$

where n(D) is the drop size distribution [Drops/$m^3$/mm diameter increment ], $V_T(D)$ is the terminal velocity [m/s] and $D$ is the drop diameter [mm]. Since the equation for terminal velocity can be approximated by $V_T \approx 4.6 \, D^{\frac{1}{2}} \, m/s$ over the range of 2.2 mm - 5 mm diameter (Snyder, 1990) and most raindrops in natural rainfall are less than 5 mm, we obtain the rainfall rate (RR) in mm/hr for drops with diameters between 2.2 - 5 mm using the mixed units favored by meteorologists:

$$\text{RR}_{11} = 2.8 \times 10^{-3} \, \pi \int_{2.2}^5 \text{n(D)} \, D^{\frac{7}{2}} \, dD \tag{3}$$

Total rainfall rate is strongly dependant on the larger drop diameters. The effort to correlate rainfall rate with sound levels therefore shifted to larger raindrops beginning with Snyder's work. Some typical drop size distributions are shown in Figure 3. They were obtained during a convective storm at Clinton Lake, IL, in October, 1982 (courtesy Nystuen) using an Distromet, LTD. distrometer with a drop diameter resolution of ±0.1 mm for diameters between 0.3 - 0.8 mm, ±0.2 mm between 0.8 - 1.8 mm, ±0.3 mm between 1.8 - 3.3 mm, ±0.4 mm between 3.3 - 4.5 mm and ±0.5 mm between 4.5 - 5.6 mm.
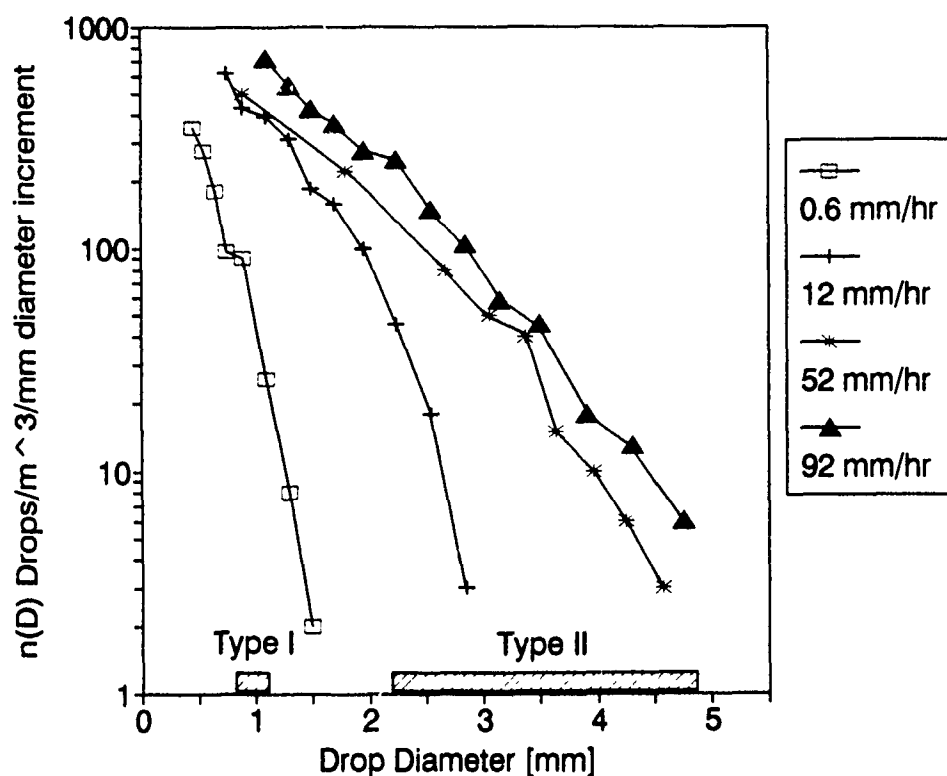
Figure 3. Typical Drop Size Distributions for Light to Heavy Rainfall (Courtesy Nystuen)

Initial investigation in the NPS laboratory of the sound produced by large, terminal velocity raindrops produced startling results (Snyder, 1990). Snyder was able to directly correlate bubble frequency with drop diameter for drops between 2.7 and 4.6 mm (5 mm is the largest drop normally found in heavy rainfall). With this knowledge, the goal of correlating rainfall rate with sound level appears to be feasible.

The goal of this thesis is to extend the results of Snyder's work to include both the energy radiated by large raindrops and the dependence of the energy radiated on the ocean parameters of temperature and salinity. With these findings, it will be possible to obtain both total rainfall rate *and* drop size distribution from the underwater sound radiated by rainfall. In addition, it will also be possible to construct an underwater rainfall sound spectrum level given only the drop size distribution. No other method is currently able to accomplish either of these tasks successfully.

## II.  EXPERIMENTAL SETUP

### A.  ACOUSTICAL EXPERIMENT

#### 1.  Drop Tower

The Naval Postgraduate School has a facility unique in raindrop sound research: a 3 m x 3 m x 26 m vertical utilities shaft with a 1.5 m deep x 1.5 m diameter redwood lined anechoic tank at its bottom (Figure 4). The top of the utilities shaft is fully accessible to allow simulated raindrops to fall through the entire 26 m travel. This distance is adequate to produce terminal speed in all sizes of drops found in normal rainfall ( < 4.8 mm diameter) as shown in previous work (Snyder, 1990). This "drop tower" was used in all portions of this research, except for the crossover energy experiment for intermediate raindrops with diameters between 1.1 to 2.2 mm.
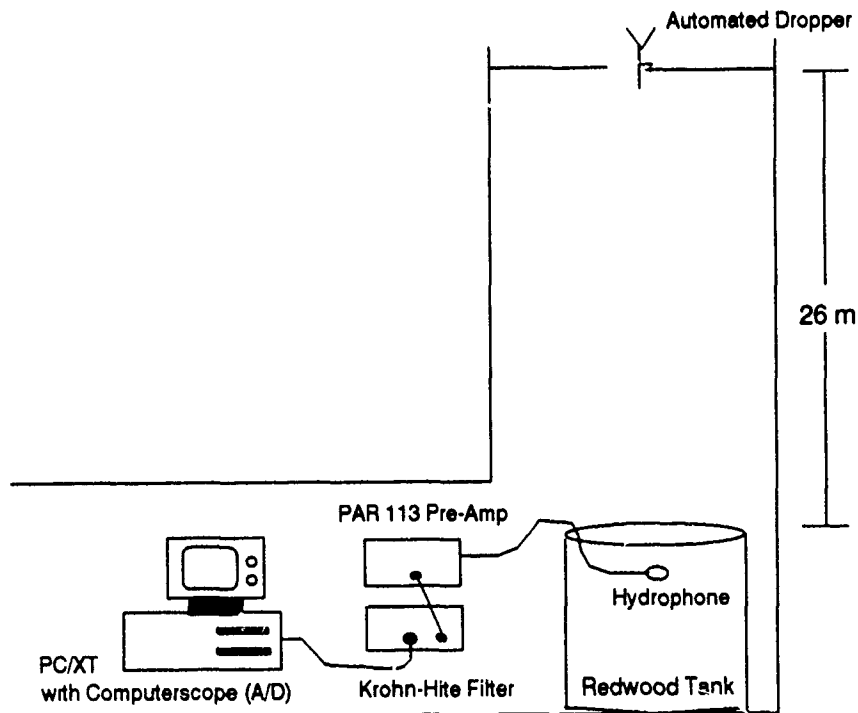


Figure 4.    Diagram of Drop Tower and Redwood Tank

## 2. Anechoic Redwood Tank

The tank used to conduct the acoustical portions of this work is a cylindrical, Winemaker's barrel with dimensions of 1.5 m height and 1.5 m diameter. Although the redwood used in the construction is known to be a good absorber of acoustic energy, an additional 15 cm of rough redwood was inserted to further mitigate the effects of reverberation. This lining was not present for the data used in Snyder's (1990) work, but the appropriate correction factors (to account for the additional reverberation) have been used for comparison. A minimum of 7 dB reduction in reverberation level at 3 kHz and up to 22 dB reduction at 20 kHz was noted when the lining was used.

The tank was filled with tap water for all portions of this work, with the exception of the salinity experiment. To simulate ocean water containing 35 ppt salinity, the tank was filled with Sea Salt, manufactured by Lake Products, Co. The temperature of the water can be maintained at elevated temperatures (up to 30 °C) by continuously running an attached filter and covering the tank when not in use.

## 3. Low Velocity Drop Apparatus

To obtain the lower (non-terminal) velocities required for the crossover energy experiment, a 3 m ladder was used to achieve a variable height above a 20 gallon fish tank. The crossover energy experiment did not require any quantitative acoustical measurements, so the reverberant nature of a small aquarium did not affect the results. The tank also provided an excellent setting for filming the impact sequence of the drop at the air/water interface during the high speed filming, discussed later this chapter.

## 4. Drop Producing Apparatus

The early work, based on the same data contained in Snyder's (1990) experiments, used several means of drop production. An Eppendorf digital pipette (Model 4710 0.5 - 10.0 μl) was used for the 2.2 - 2.7 mm drop diameter range, with a published volume accuracy of ±1%. For drops in the range of 2.7 - 3.6 mm diameter, an Eppendorf digital pipette (Model 4710 10 - 100 μl) was used, with a published volume accuracy also of ±1%. For drops with a diameter greater than 3.6 mm, individually calibrated glass eye droppers were used. The accuracy of the eye droppers was calculated by measuring the volume of 50 drops at least 5 times (collected in a graduated cylinder) and was measured to be ±5% by volume. The acuracy of the graduated cylinder was ± 0.1 ml. For example, a 4.6 mm drop has a volume of 50 μl, therefore 50 drops should have a volume of 25 ml. In all cases of volume measurement, the volume of the 50 drops was

7

within 1.2 ml, or 5%. The accuracy was also verified on an Ohaus precision balance to be ±5% by mass *for each individual drop*.

In the later work, a smaller range of drop sizes led to the automation of the drop producing process. A standard medical intra-venous drip bag was used to feed a calibrated glass eye dropper that produced a stream of separated drops with an adjustable drop rate. This freed one person from the task of creating hundreds of drops at a sitting and minimized the drop strike radius by maintaining a constant "aim." The repeatability of the droppers was calculated by measuring the volume of 100 drops at least 5 times and was ±5% of the expected volume for all drop diameters used. Again, the accuracy was verified using an Ohaus precision balance to be ±5% by mass *for each individual drop*.

## 5. Hydrophone

The construction of the hydrophone was similar to that of an LC- 5 and consisted of two 1/8 inch coaxial cylindrical barium titanate elements. The hydrophone was calibrated by both the spherical reciprocity and comparison calibration methods. Its response was quite flat (± 1.5 dB) up to 50 kHz and ±5 dB from 5 - 300 kHz (Figure 5 on page 9). It was positioned at 15 cm depth for the early work and 6 cm depth for the later work. Although the shallower depth included the near-field acoustic and hydraulic effects experienced during an impact, the increased signal to noise ratio provided a much cleaner signal. Also, the near field effects can be accounted for, as described in Chapter IV.
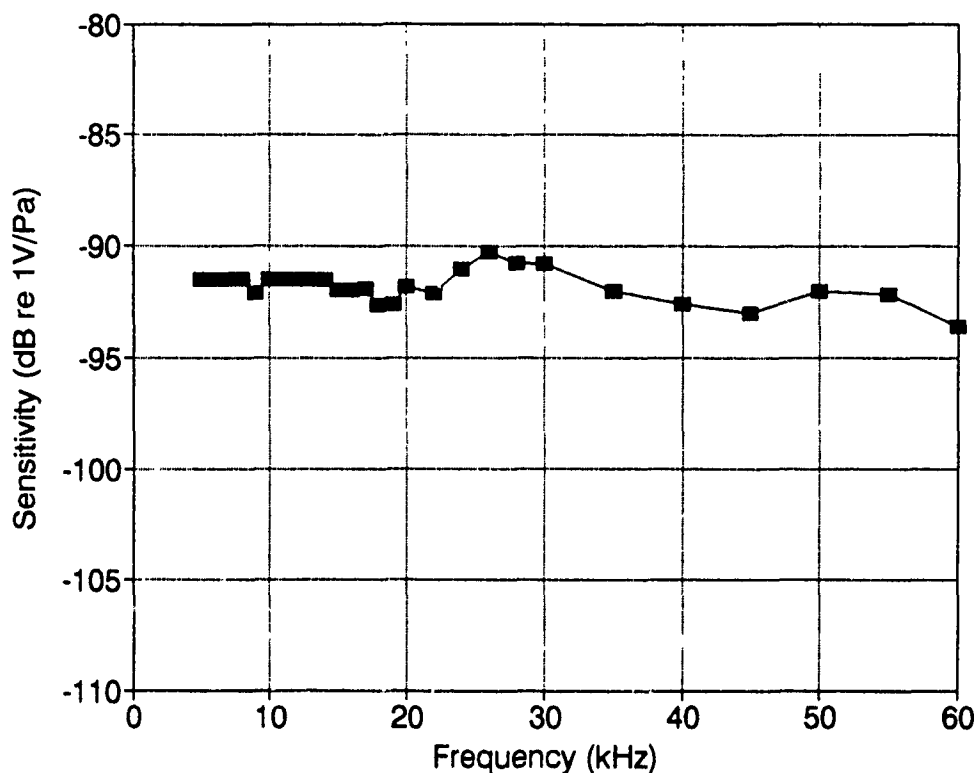
Figure 5.  Hydrophone Calibration Curve

### 6.  Amplification and Filters - Early Work

The signal from the hydrophone was amplified by a PAR 113 Low Noise Pre-Amplifier with a gain of 2000 for drop diameters greater than 3.4 mm and 10,000 for drop diameters less than 3.4 mm.  It was then passed through two Krohn-Hite band pass filters with a pass frequency band of 2 kHz to 30 kHz.  This gave a total roll-off of 48 dB per octave, which was necessary due to large amounts of interference at 1800 Hz (caused by ventilation fans) and 31.25 kHz (produced by an unknown source in the building).

### 7.  Amplification and Filters - Later Work

The later work was conducted during a portion of the year that was less noisy and included an isolation transformer for the filters which minimized the 60 Hz ventilation fan noise.  The PAR 113 Pre-Amplifier was used at a gain of 2000 for all drop diameters.  The signal was then fed to a single Krohn-Hite 3202R band pass filter,

9

passing frequencies between 1 Hz - 300 kHz for impact signal acquisition and 1 kHz to 30 kHz for bubble signal acquisition. These band pass frequency ranges contain at least 99 % of the total signal energy as determined by conducting trials both with and without filtering.

## 8. Data Acquisition

A digital data acquisition card, Computerscope, marketed by RC Electronics, was mounted in an IBM PC/XT and was used for data acquisition in all acoustical experiments. It is capable of sampling frequencies of up to 1 MHz at an amplitude resolution of 12 bits. It could sample up to 16 channels simultaneously, but the maximum sampling frequency would be lowered. The temporal resolution given by the 1 MHz sampling frequency was helpful when small time differences were measured from isolated impacts. A lower frequency of 250 kHz was selected for all of the bubble data samples, since a longer record length was needed than could be achieved at higher sample frequencies.

## 9. Distance Measurements

The early work used a video camera / tv monitor setup to measure the horizontal range from the impact to the hydrophone with an accuracy of $\pm$ 1.5 cm. In the later work, distance was measured directly with a ruler, leading to an accuracy of $\pm 0.5$ cm.

## 10. Temperature Measurements

Several Navy-issue thermometers were used in this work with an overall range of -20 C to +50 C. Accuracy was $\pm$ 0.5 C.

## 11. Salinity Measurements

The salinity content of the water used for the saline dependence experiment was measured by an AGE Model 2100 Salinometer with an accuracy of 0.05 ppt.

## B. PHOTOGRAPHIC EXPERIMENT

### 1. High Speed Photography

Motion pictures of terminal speed 4.6 mm drops impacting the water surface were taken in conjunction with both this work and Snyder's (1990) work. A 400 frame per second Milliken camera was used to capture the time sequence from the initial impact through the violent tearing of the canopy. A complete analysis of this experiment is given in Snyder (1990) and is reviewed in this work in Chapter IV.

## 2. Video Camera Photography

In the crossover energy experiment, it was necessary to see the cavity formation sequence for several velocities of a given drop size. This was accomplished with a Sony CCD-V99 video camera recorder. A 650 W movie light was used to provide adequate light to allow the use of a 1/1000 s shutter speed. This high speed was necessary to stop the motion of the crater formation. A 20 cm depth of field was possible when using the 'macro' mode of the lens. The setup used is shown in Figure 6.
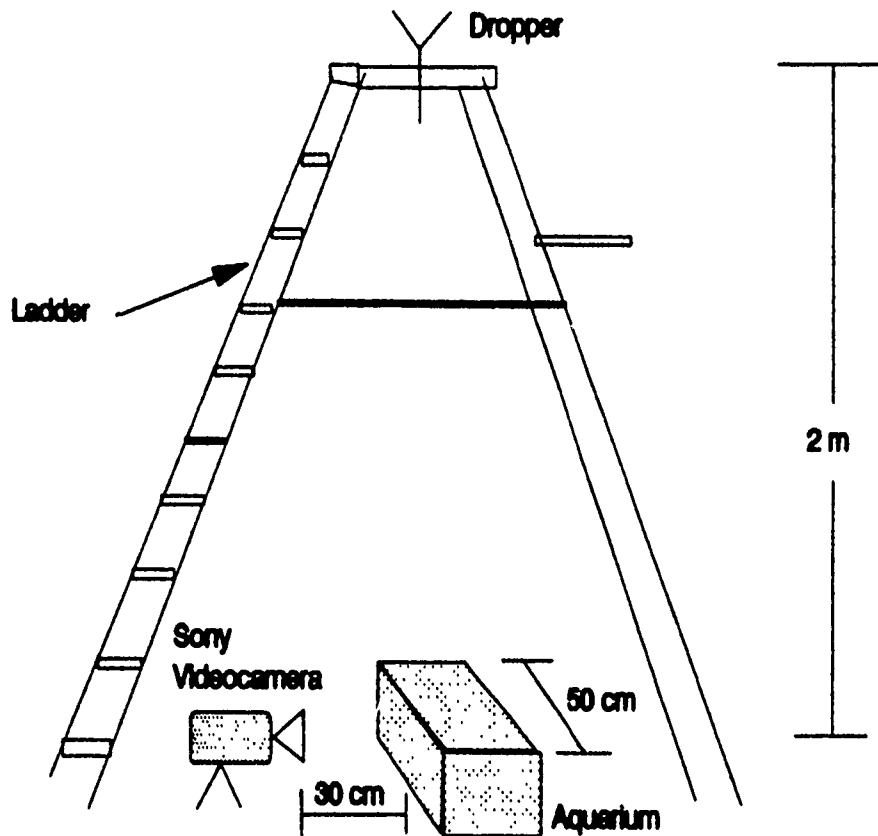


**Figure 6.    Setup Used for the Crossover Energy Determination**

# III. NUMERICAL ANALYSIS METHODS

## A. INITIAL CALCULATIONS

### 1. Signal Input

The recorded acoustic energy was sampled at the predetermined time interval using the Computerscope data acquisition card. The digitized input has an amplitude resolution of 12 bits and is recorded as a voltage level which ranges between $\pm 10$ V. This voltage level is proportional to the pressure at a range determined by the geometry of the hydrophone and drop impact position.

### 2. Correction to 1 m on Axis

Both the impact and bubble signals were then corrected to an equivalent pressure which would be at 1.0 m and on the vertical axis below the drop impact point. This correction must take into account the $1/r$ spherical spreading as well as a $\cos \theta$ dependence as shown in Figure 7. This latter correction assumes that both the bubble and impact behave as acoustic dipoles. The bubble radiation pattern has been confirmed for smaller, terminal velocity drops at normal incidence (Kurgan, 1989). If the original voltage amplitude is given by A [v], then the correction factor is:

$$A_{at\,1\,m\,on\,axis} = A \times \frac{h^2 + z^2}{100\,z} \tag{4}$$

where z is the depth of the hydrophone in cm and h is the horizontal distance from the hydrophone to the drop impact point in cm.
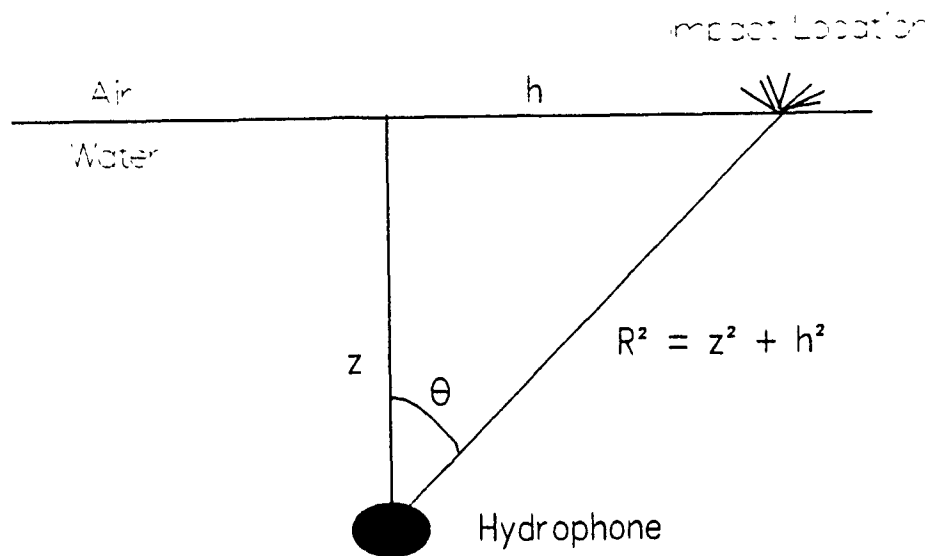
Figure 7.    Geometry for Dipole Correction for Range and Angle

## 3.  Near Field Correction

The near field effect caused by being within several wavelengths of a dipole causes an error between the measured pressure field and the extrapolated (at 1 m) pressure field.   The proper correction factor has been derived to be (Medwin and Beaky, 1989):

$$A_{\text{at 1m on axis far field}} = A_{\text{at 1 m on axis}} \cfrac{1}{1 + \cfrac{1}{k^2 R^2}} \qquad (5)$$

where k is the wave number in $m^{-1}$ and R is the range from hydrophone to impact in m.  In further equations, a prime superscript will be used to denote "at 1 m on Axis, Far Field."

The near field correction was not made for the earlier work due to the hydrophone placement at a depth of 15 cm, which is at least one wavelength from the surface for all frequencies above 10 kHz.  These measurements were taken in the redwood tank before the anechoic lining was installed, and the reverberation clearly dominated any errors introduced by the near field values.

The later work required the near field correction since all frequencies of interest were in the near field at a hydrophone depth of 6 cm.

13

## 4. Fourier Transform

The temporal signal was converted to its frequency components by a 2048 point Fast Fourier Transform. The routine used (from the Borland Turbo Pascal Numerical Toolbox) was based on the Cooley-Tukey method and is given by:

$$X(k) = N^{-1/2} \sum_{k=0}^{N-1} x(n) e^{-i2\pi nk/N} \tag{6}$$

Some methods of FFT do not include the $\sqrt{N}$ in the forward transform and use a $1/N$ term in the inverse transform instead. Also, a factor of $\frac{1}{2\pi}$ may differ between this method and others. These factors are the most likely reason why results obtained from another source may differ slightly with the results presented in this paper.

The unit analysis continues:

$$A'\left[ \frac{V}{\sqrt{\text{Bin Width}}} \right] = \text{FFT} \left( A'[V] \right) \tag{7}$$

where bin width is given by

$$\text{Bin} Width[\text{Hz}] = \frac{F_s}{2048 \, [Bins]} = \frac{250,000 \, [Hz]}{2048 \, [Bins]} = 122 \, [Hz/Bin] \tag{8}$$

The sensitivity of the hydrophone is uniform over the frequency range of interest and has a value of -91.5 dB re 1V/Pa. This is equivalent to 37,580 Pa/V.

With this information, the desired result of spectral density for a 1 Hz bandwidth at 1 m on axis in the far field can be obtained. For simplicity, these conditions will be denoted by a double prime superscript. For a case with a gain of 2000,

$$A''\left[ \frac{Pa^2}{Hz} \right] = \frac{1 \, \text{Bin Width}}{122 \, [Hz]} \left( \frac{37580 \, [Pa/V]}{2000[V/V]} \right)^2 A'\left[ \frac{V}{\sqrt{\text{Bin Width}}} \right]^2 \tag{9}$$

The result of this calculation is the spectral density from a single bubble or impact.

## B. DATA ANALYSIS PROGRAMS

### 1. Single Drop Processing

All of the initial calculations were carried out by a single program written to run in batch mode (no user interaction). Each bubble and impact were processed sequentially and yielded an output of frequency versus spectral level [Pa/$\sqrt{Hz}$]. Each individual

14

spectrum was evaluated for noise levels, peak frequency, and the presence of secondary bubbles and atypical signals. The duration of the bubble record was fixed at 8.2 ms to establish a standard record length for subsequent processing and was based on the shortest record length able to capture at least 99% of the energy from the bubbles produced by the 4.6 mm drops. The impact record length was set at 256 microseconds, long enough to capture the impact for all drop diameters.

### 2. Multiple Drop Processing

The spectral densities of a number of bubbles or impacts with a common parameter (drop diameter, temperature or salinity) were averaged by a second, user-written program. The output of this program is frequency versus spectral density $[Pa^2/Hz]$, which can then be plotted or used for energy calculations. The reasons for requiring an average value are discussed below.

### 3. Plotting

The results from the averaging program were plotted using Quattro Pro, which was selected for its versatility in vector (column) calculations and rich graphic capabilities. For each set of data, the total spectral density is calculated by adding the spectral density from the impact together with a fraction of the spectral density from the bubble. This ratio takes into account that impact energy is produced with each raindrop strike, while bubbles are created and radiate energy for only a fraction of the drops.

## C. DATA AVERAGING

Due to the natural variability in sound spectrum shapes produced by impacts and bubbles, it is necessary to view the results using statistical techniques. No raindrop will produce a spectral shape *exactly* like another. It is therefore necessary to average the bubble and impact spectrums in both frequency and ensemble. The frequency average consists of a 1 kHz wide moving filter applied to smooth the individual spectrum before plotting. The ensemble average uses all drops of a similar category (e.g., all 4.6 mm drops). Also, the standard deviation of the spectral levels at the dominant bubble frequency is given, as well as the standard deviation of the total energy per raindrop, to present the reader with a good measure of the variability of energy present in rainfall.

## D. ADDITIONAL CALCULATIONS

### 1. Average Spectral Energy per Raindrop

To obtain the spectral energy per raindrop, the frequency dependant average spectral density $[Pa^2/Hz]$ at 1 m on axis due to a given diameter of raindrop (or other parameter) is integrated with respect to frequency. The integration will yield the square

of the pressure radiated by that average raindrop. Assuming a dipole radiation pattern, this can then be converted to spectral intensity on axis and integrated by using ring elements $[(2\pi R \sin\theta)\, R\, d\theta]$ over the area of radiation. It follows that

$$\frac{Energy(f)}{Drop\ Time} = \left(2\pi\frac{R^2}{\rho c}\right)\int_0^{\frac{\pi}{2}} A'' \cos^2\theta \sin\theta\, d\theta \tag{10}$$

which, for $R = 1$ m yields

$$\frac{Energy(f)}{drop} = \frac{2\pi}{3\rho c}\, A'' \times Time \tag{11}$$

where *Time* is given by the length of time the bubble radiates sound. For this analysis, the time will be the record length of data extracted to meet the requirements of the FFT algorithm (# of data points is a power of two) and has been chosen to be 8.2 ms. A record length of 8.2 ms has been shown in the laboratory to capture at least 99% of the total energy radiated by a typical bubble.

## 2. Calculated Underwater Sound Spectrum Levels due to Rainfall

For a known drop size distribution, it is possible to use the average spectral density at 1m on axis per raindrop computed previously to obtain the calculated rainfall spectrum, RS(f), for the given drop size distribution. This is a straightforward calculation:

$$RS(f) = \sum_D A''\ RR(D)\ T_s\ Area\ \frac{1^2}{(Effective\ R)^2} \tag{12}$$

where RS(f) has units of $Pa^2/Hz$, $A''$ has units of $Pa^2/Hz\ /drop$, $RR(D)$ is the rainfall rate $drops/m^2\ s$ of diameter D and $T_s$ is the total sample time used for data collection (8.2 ms for this experiment). The effective R is determined by the location of the raindrop with respect to the hydrophone, taking into account the dipole radiation pattern of the raindrop. This calculation allows one to compare the theoretical results with previously measured spectrum levels if the hydrophone geometry is known. An example will be shown in Chapter VI.

16

# IV. DESCRIPTION OF RAINFALL MECHANISMS WHICH CAUSE BUBBLE FORMATION

## A. TYPE I MECHANISM

### 1. Background

Bubbles generated by the Type I raindrop mechanism have been previously defined (Snyder, 1990) as those bubbles caused by terminal velocity drops sized from 0.8 mm to 1.1 mm diameter. Bubbles of this mechanism are the primary component of low rainfall rate and occur during light wind and at near normal incidence (Nystuen and Farmer, 1987). They produce a spectrum with a sharp peak centered at about 15 kHz. This peak has been shown to broaden and weaken as wind speed increases, due to a lower production rate of bubbles when drops impact at oblique incidence (Kurgan, 1989; Medwin, et al.,1990; Nystuen, 1991).

The range of terminal velocity drops that produce Type I bubbles is shown in Figure 8. This figure shows all of the previously identified regions of bubble production. The curves labeled "NCPA" have been described by the National Center for Physical Acoustics in Mississippi (Pumphrey and Elmore, 1990). Most of the work done by NCPA has been away from the terminal velocity curve. Since rain always falls at terminal velocity, research conducted away from the terminal velocity curve does not represent rainfall at sea.

17
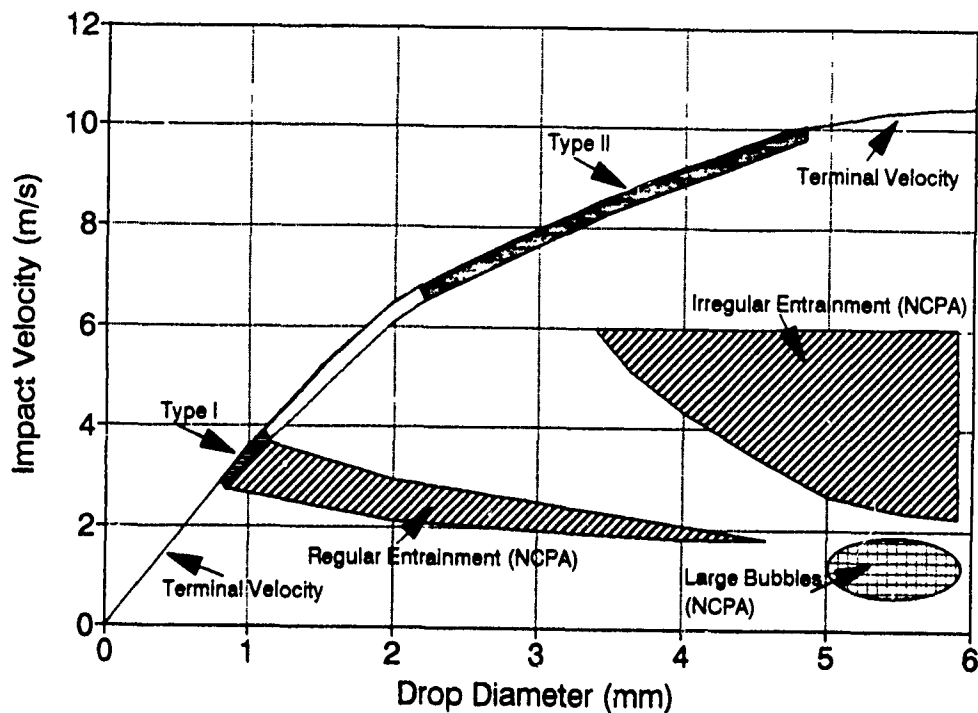
**Figure 8.** Known Bubble Production Regions

## 2. Bubble Production Mechanism

Type I bubbles caused by drops falling at terminal velocity have been thoroughly researched both experimentally (Kurgan,1989; Pumphrey, et. al.,1989; Medwin, et.al. 1990) and theoretically (Oguz and Prosperetti, 1990; Longuet-Higgens, 1990). The exact mechanism of bubble production is not known, but several theories present likely conclusions.

After the impact of the drop, a conical cavity is formed. The shape of the cavity is the key visual identification of the Type I mechanism. For a small range of drop sizes at terminal velocity (0.8 - 1.1 mm), a bubble is pinched off at the bottom of the cone after a variable delay time of about 20 ms. This pinch-off may occur because of capillary waves that join at the bottom of the conical surface (Longuet-Higgens, 1989). This theory states that the pinch-off will occur when the conical angle reaches 109.5 degrees.

18

Another possible explanation is that the bubble is pinched off when the conical cavity forms a "nipple" at the bottom (Oguz and Prosperetti, 1989). Under certain geometrical conditions, this "nipple" separates from the cavity to form a small bubble.

Both of these theories require a delicate geometrical structure to allow creation of a bubble. However, when a drop strikes a flat surface at oblique incidence, which is equivalent to a drop falling against a wave at other than normal incidence, the percentage of bubbles produced decreases rapidly (Kurgan, 1989; Medwin, et. al., 1990). All theories support the conclusion that a bubble is pinched off only when symmetrical conditions apply. Results from rainfall studies also show that when wind speed increases (causing oblique incident angles), the characteristic 15 kHz peak created by Type I bubbles decreases in amplitude and becomes broader in the frequency domain.

The Type I mechanism (pinch-off) has also been observed in drops at velocities other than terminal velocity (Pumphrey, 1989). These drops are described by the "regular entrainment" region of Figure 8 and exhibit a similar 15 kHz peak. Drops in this region do produce bubbles 100% of the time but are not useful in the study of rainfall, since rain is comprised of only terminal velocity drops. However, bubbles produced by drops in this region may be commonly present in the ocean due to the spray from waves or as secondary bubbles during heavier rainfall.

## B. TYPE II MECHANISM

### 1. Background

Bubbles caused by the Type II mechanism have been previously defined (Snyder, 1990) as those dominant bubbles caused by terminal velocity drops ranging in size from 2.4 mm to 4.6 mm diameter (Figure 8). This paper broadens the definition to include terminal velocity drops between 2.2 mm and 4.6 mm and secondary bubbles as well. Bubbles produced by this mechanism were first studied by Franz who stated, "The bubble component of the underwater sound energy from the splash of a water droplet is very erratic under most conditions." (Franz, 1959) This notion of unpredictability was carried on by Pumphrey and Crum in 1989 when this mechanism was labeled "irregular entrainment."

Recent work has shown that although a wide varie., of drop size / impact velocity combinations will form bubbles by the Type II mechanism, statistically predictable results can be obtained when terminal velocity drops (rainfall) are investigated (Snyder, 1990).

Results presented later show that formation of a dominant bubble varies from 0% at the low end of drop sizes researched (2.2 mm diameter) to a peak of 65% at approximately 4.2 mm diameter. Drops above 4.6 mm diameter were not considered, as Nature rarely produces drops larger than these. The frequency of the dominant bubble produced by this mechanism can be directly related to drop size (Snyder, 1990), which indicates that 2.2 mm to 4.6 mm drops falling at terminal velocity are good candidates for estimating the distribution of raindrop sizes by acoustic means. A typical time domain sequence of a dominant bubble created by a Type II mechanism is shown in Figure 9.
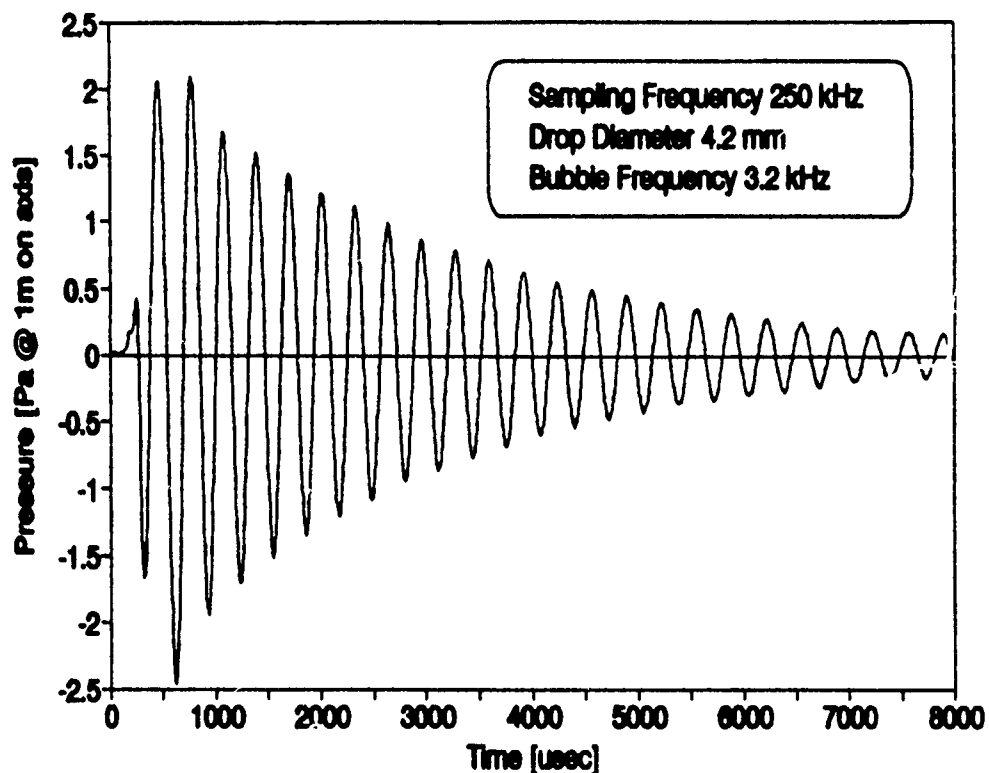


Figure 9. Time Domain Portrait of a Dominant Bubble

## 2. Bubble Production Mechanism

Although Franz had photographed the Type II mechanism in 1959, only recent photographic efforts described by Snyder have identified the sound producing components of this mechanism. Sketches from the high speed photography work are shown in

Figure 10 for a 4.7 mm drop (Snyder, 1990). The time between frames is 2.5 ms, although the frames shown are not necessarily consecutive.

The first frame shows the drop slightly prior to impact. Note that the drop is not spherical but is flattened on the bottom. This shape has been predicted theoretically (Pruppacher and Pitter, 1971).

The next frame shows the formation of the crown and the beginning of a hemispherical crater in the water, which begins shortly (2 ms) after impact. Note the spray of aerosols ejected by the upward travelling water mass. The next several frames show the closing of the canopy, most likely due to surface tension. The canopy closes about 15 ms after the impact.

After the canopy closes, a jet of water continues to rise from the site at which the canopy closed. The next frames show the growth of the canopy to a height of 2.9 ± 0.3 cm at a time of 25 - 30 ms after impact. When the jet has reached a peak in height, a downward moving jet appears at the base of the upward moving jet. This jet plunges downward towards the bottom of the flattened crater with an observable cant (angle).

The next frame shows the jet piercing the bottom of the flat-bottomed crater. Several ms later, a bubble is broken off from the tip of the turbulent jet, apparently due to buoyant forces that act on the air trapped in the tip of the jet. Delay times from the impact to the onset of the bubble range from 35 ms to 65 ms and depend on drop diameter (Figure 11).

The jet then retracts into the crater, which is already in the process of collapse. The canopy remains on the surface for 20 - 50 ms before tearing itself apart, violently spraying aerosols as far as 5 cm from the point of impact.

From the photographic evidence seen, the necessary criterion for bubble formation is the cant of the turbulent jet as it plummets downward through the crater. If the jet is perpendicular to the water surface, no buoyant forces are exerted, and no bubble is produced. It is believed that drops incident at oblique angles would have a higher percentage of bubble production. From a simple geometric standpoint, it can be argued that oblique incidence would provide the imbalance that is necessary for bubble production. Wind, therefore, should enhance the spectrum produced by this Type II drop mechanism. This is in direct contrast to the Type I mechanism, which shows a decrease in bubble production in the presence of wind.
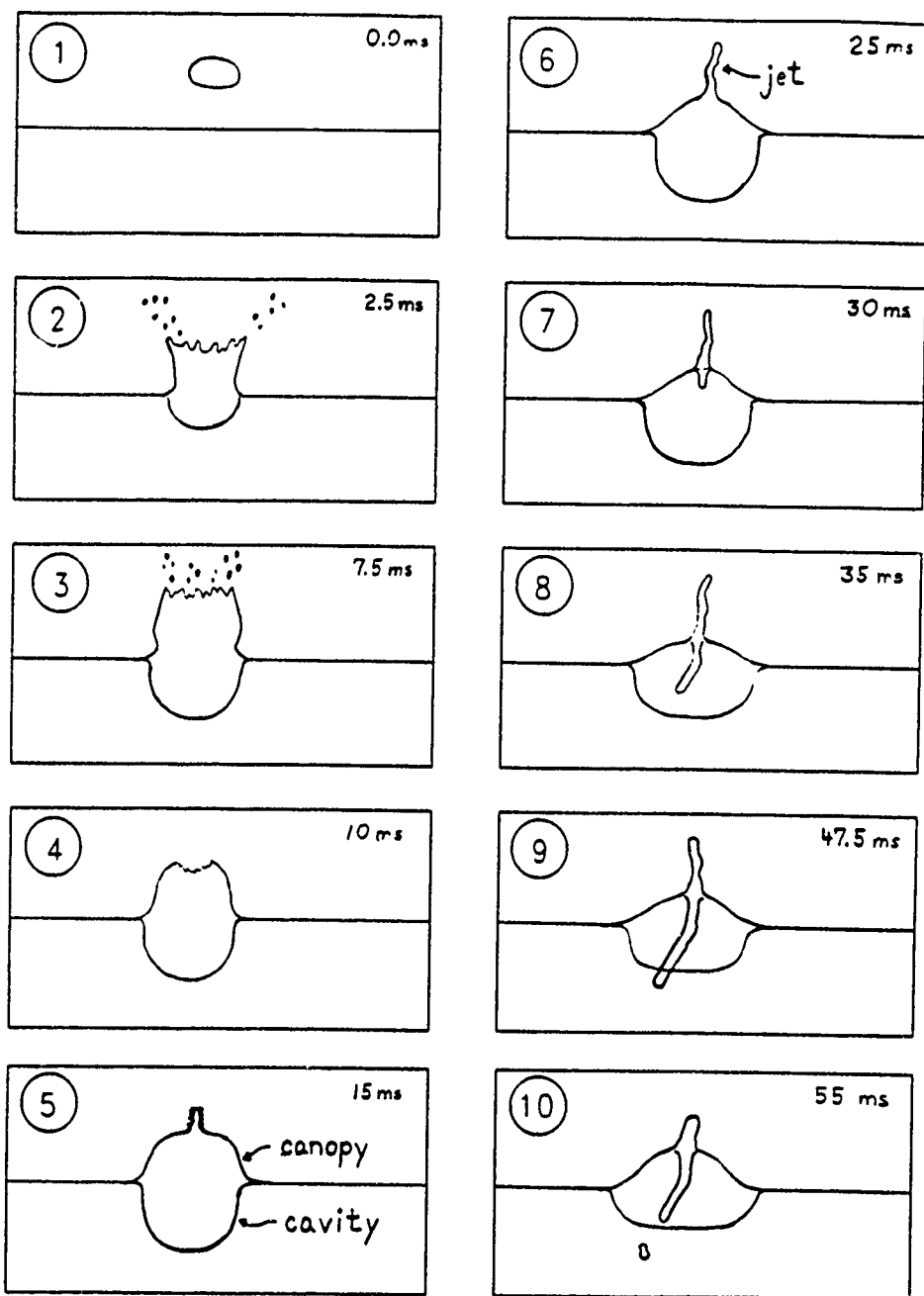
Figure 10. High Speed Photographic Sequence of Type II Mechanism
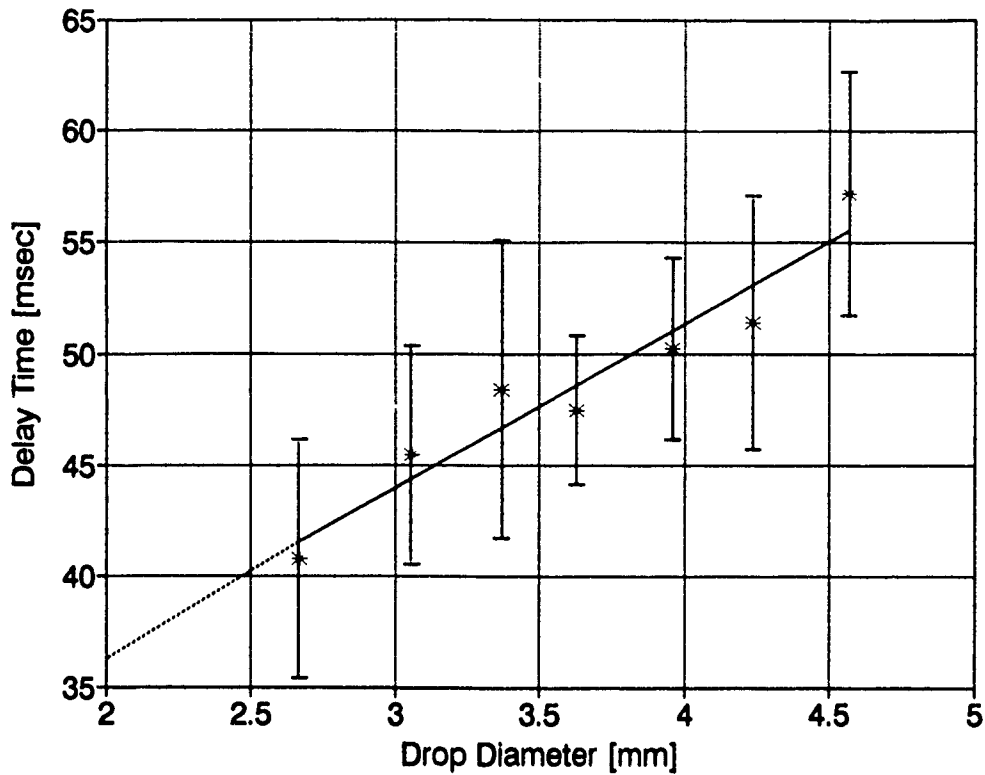
Figure 11.    Delay Time From Impact to Onset of Bubble

## 3.  Secondary Bubble Production

In a small number of cases, a second, smaller bubble is produced by the Type II mechanism. A time domain example of this is shown in Figure 12. This phenomenon deserves attention because of the energy potentially contributed by the secondary bubbles to the overall spectrum.
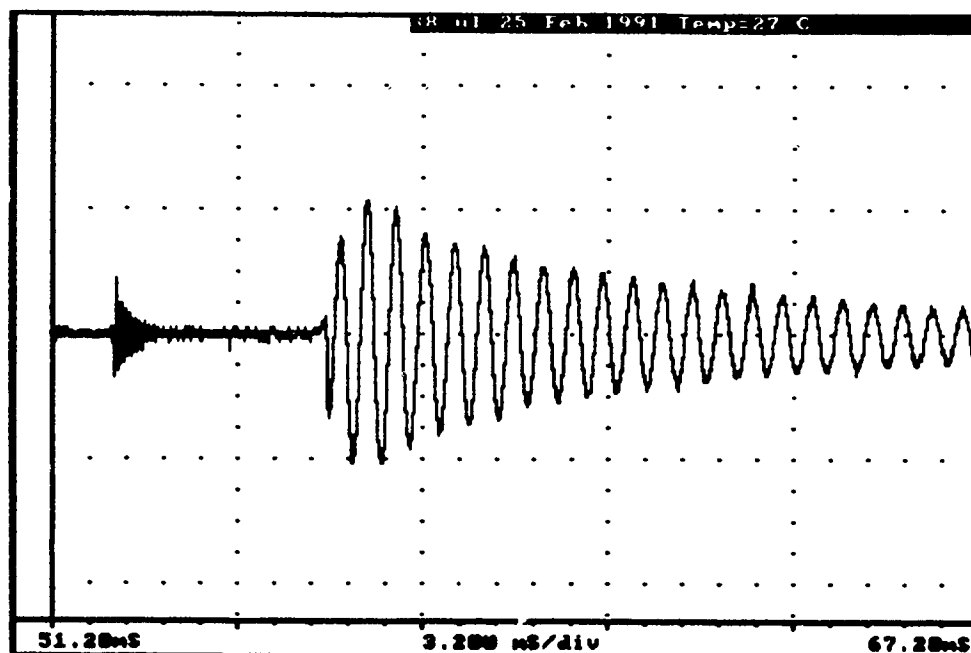
**Figure 12.** Time Domain Portrait of a Secondary Bubble Which Precedes a Dominant Bubble

## 4. Wobble Production

In a moderate number of cases (more fully described in the next chapter) a strange phenomenon resembling a gated sinusoid appears (Figure 13). This phenomenon has been labeled a "wobble" because of its appearance. The mechanism of sound production has not been identified, but it may be related to pulsations of the turbulent jet or caused by capillary waves modulating the jet. The wobble has been observed both before and during the dominant (as opposed to secondary) bubble. On several occasions the wobble has been the only source of sound.

The start of the wobble is very abrupt, as is its end. The start has been observed as early as 16 ms after impact, and as late as 1 ms prior to the dominant bubble (the dominant bubble delay time is a function of drop diameter). It maintains an almost constant amplitude during the entire event, which can last between 5 - 13 ms, and has approximately the same duration as the dominant bubble. The amplitude, however, remains constant and does not show an exponential decay, as does the bubble. The wobble has been investigated to determine the amount of energy contributed (Chapter V). In addition, the frequency of the wobble and its entire spectrum has been examined

24

to see whether one can separate the wobble from the dominant bubble in the frequency domain (Chapter V).
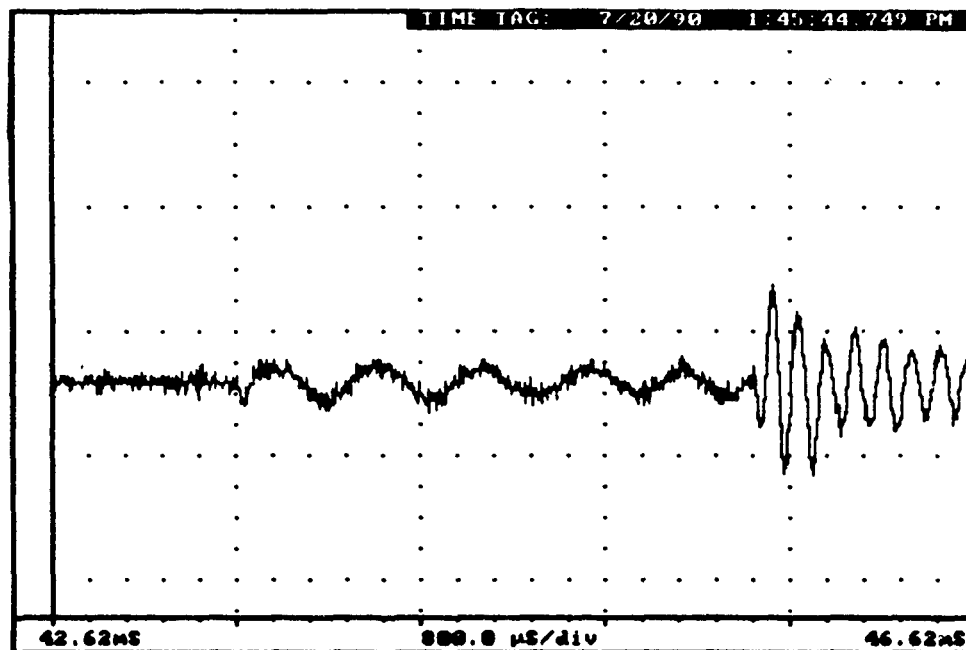


Figure 13.    Time Domain Portrait of a Wobble (starts at 43.4 ms and continues into
the dominant bubble)

## C.  CROSSOVER KINETIC ENERGY

### 1.  Background

Franz theorized that the difference between the two mechanisms that he had seen (non-terminal velocity experiments which we assume were Type I and Type II) was based on drop velocity. It is easy to see from other work, such as the photographs in Pumphrey's (1989) dissertation, that velocity is not the only criterion. This is also evident from the regions identified by NCPA (Figure 8). A possible alternative to velocity is the drop's kinetic energy at impact.

### 2.  Experimental Setup

To test the theory that kinetic energy is the critical parameter for type II bubble creation, several readily available points of data were used. Our research has shown that

a terminal velocity 2.2 mm drop produced a bubble from the Type II mechanism 0% of the time. Drops larger than 2.2 mm diameter falling at terminal velocity often produced bubbles. It was therefore assumed that the 2.2 mm drop possessed the minimum kinetic energy necessary to initiate the Type II mechanism.

Our postulate was that if a drop larger than 2.2 mm, falling at a lower velocity, had the same (or less) kinetic energy as the 2.2 mm drop at terminal velocity, the Type II mechanism would not be present. If the drop were released from a higher point (giving a larger kinetic energy) the Type II mechanism would be seen. If the drop were released from a lower point, the Type I mechanism would be seen (see Figure 8).

The 5.2 mm drop diameter was selected for this experiment because of the availability of eyedroppers that yielded this drop size. 100 drops were released from 2.15 m and had a calculated velocity of 5.4 m/s at impact (corresponding to the NCPA "irregular entrainment mechanism"), using the formula (Pumphrey, 1989):

$$v = v_T \sqrt{1 - e^{-\frac{2gz}{v_T^2}}} \tag{13}$$

where $v_T$ is the terminal velocity of the drop. Drops were also released from 0.25 m (corresponding to the lower kinetic energy of the Type I "regular entrainment region") to check for the Type I mechanism. These lower velocity drops had a calculated impact velocity of 2.2 m/s. A video camera was used to provide a record of the experiment as well as to provide frame-by-frame playback capability to study the drops.

## 3. Results

At 2.15 m height of release, several of the characteristic Type II mechanisms were noted for the 5.2 mm drop (velocity 5.4 m/s). The hemispherical crater and crown were easily seen. The remainder of the drops formed another structure, unlike Type I or Type II, which did not appear to produce bubbles. This type of drop splash has been noted previously by Franz and was identified as the "third type" (Franz, 1959).

At a height of 0.25 m the results for the 5.2 mm drop (velocity 2.2 m/s) were quite different. Most of the drops had the characteristic conical shape of the Type I mechanism, and no Type II mechanisms were noted. Several of the drops had the "third type," which may be an intermediate structure between Type I and Type II.

However, further investigation yielded similar results for the 5.2 mm drop at a height of 1.25 m (corresponding to an impact velocity of 4.6 m/s). From Figure 8, only the Type II mechanism should be present at this velocity. The corresponding kinetic energy is well above that of the 2.2 mm drop at terminal velocity.

26

These results appear to support the claim made by the NCPA that the region labeled "irregular entrainment" in Figure 8 is indeed properly labeled for *non-terminal velocity* drops. There *does not* seem to be a clear, unique dividing line of kinetic energy separating the Type I and Type II mechanisms for all drop diameters and all velocities.

# V.  IMPACT AND BUBBLE ENERGY ANALYSIS

## A.  ENERGY SOURCES

The energy radiated into the water by a drop splash consists of four primary elements: Impact sound, underwater hydrodynamic motion, surface wave generation and bubble sound radiation.  Only two components, impact and bubble sound radiation, are of present interest.  Hydrodynamic effects, however, can contribute substantially to the overall near field pressure, especially for the impact water hammer followed by the generation of the crater.  The subject of impact hydrodynamics continues to be researched at this laboratory.

## B.  SAMPLE SPACE

A total of 202 drops which produced bubbles and the corresponding impacts were analyzed.  Drop temperature and surface temperature were at 20 °C (room temperature) and fresh water was used.  The distribution of drop sizes is given in Table 1.  The 2.6 mm drop data was not used in further analysis due to the small sample space.  Other drop sizes (except the 3.7 mm diameter) had a standard deviation of peak bubble frequency (frequency at which the spectral density peaked) of less than 500 Hz (Snyder, 1990).  The 3.7 mm diameter had a standard deviation of 1 kHz.  The selection of approximately 30 drops of each size was based on the desire to obtain a large enough sample space to estimate the standard deviation of the dominant bubble frequency.  The selection criterion was based on data obtained for previous work (Snyder, 1990) and is adequate for this work.

Drop sizes were fixed by the availability of eye droppers and the desire to obtain a difference of about 0.3 mm between each drop diameter.

## C.  IMPACT ENERGY

### 1.  Impacts of Small (0.8 - 1.1 mm) Drops

The impact would be expected to contribute to the overall energy radiated by a drop, since the impact noise is present for each drop strike.  The impact energy of small (1 mm) raindrops has been previously investigated (Kurgan, 1989).  As expected, the radiated impact energy from this size of drop was small, on the order of 0.01 picoJoules.  Kurgan's impact spectrum for small drops peaked at approximately 15 kHz and had a -3 dB bandwidth of about 14 kHz (Figure 14).  The wide spectrum was expected, as the

**Table 1.  DROP DIAMETER SAMPLE SPACE**

| Drop Diameter (mm) | Number of Drops |
|:---:|:---:|
| 2.6 | 3 |
| 2.7 | 29 |
| 3.1 | 36 |
| 3.4 | 33 |
| 3.7 | 14 |
| 4.0 | 28 |
| 4.2 | 29 |
| 4.6 | 30 |

short duration of the impact (typically 50 - 100 $\mu$sec) in the time domain translates into a broad spectrum in the frequency domain.  However, the appearance of the peak in Kurgan's work is due to the impact spectrum not being corrected for the high and low pass filters used (as noted by Kurgan).  When corrected, the spectrum has a trough at about 6 kHz and then has an increasing magnitude with with decreasing frequency, as opposed to that shown in Figure 14.  This characteristic of the impact has been described by Pumphrey (1991) and has been experimentally verified for other drop diameters in this laboratory.

0

11.8 kHz

-3 ....8.7/ 16.6 kHz

dB

-50

0.0           10 kHz/DIVISION          80 kHz
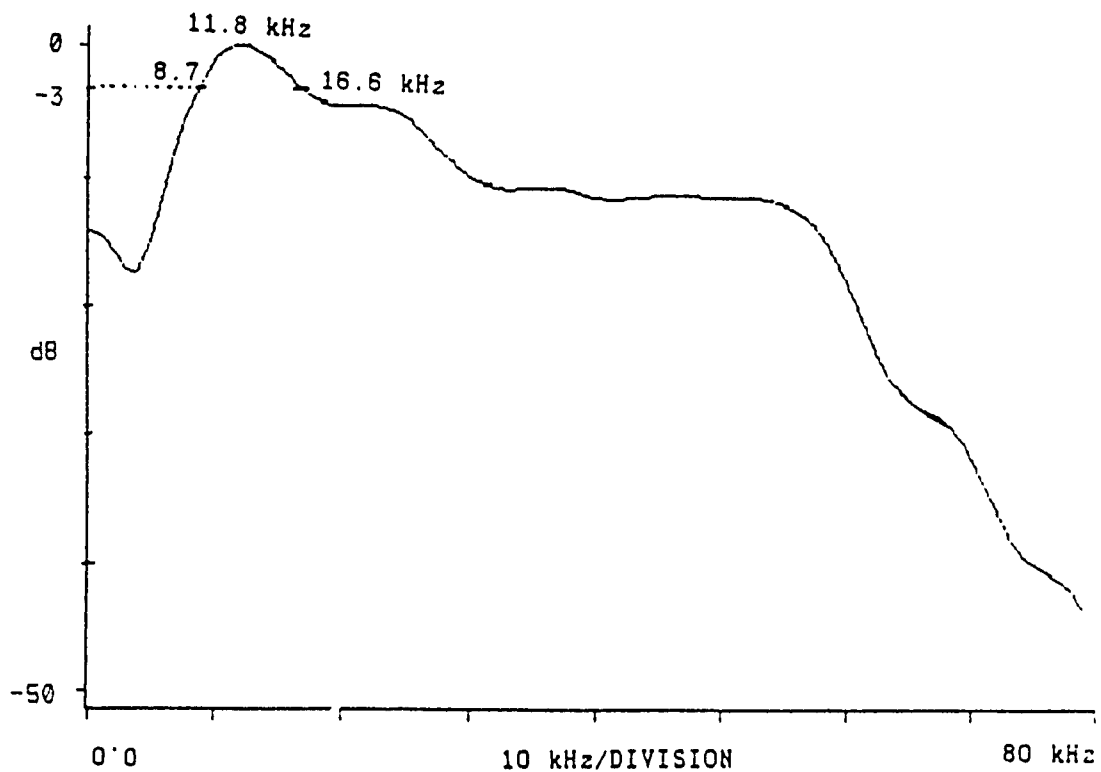
**Figure 14.** **Impact Spectrum of 0.83 mm Diameter Drop** as given by Kurgan (1989)

## 2. Impacts of Mid-size (1.1 - 2.2 mm) Drops

Impact energy is dominant in the region that bridges the gap between Type I and II bubble producing regions due to the lack of bubble production. The spectral density has a measured magnitude of about $1 \times 10^{-9}$ $Pa^2/Hz$ at 10 kHz.

Because of the monotonically decreasing shape of the impact spectrum, one must pick a reference point rather that a peak value to compare one drop with another. For comparison of the spectral densities of different drops, we use the spectral density at 10 kHz (a mid-band [0 - 20 kHz] reference point). Although this energy is much less than that for larger drops, it is a significant source of impact energy because of concentration of raindrops of this size in natural rain (Figure 3).

## 3. Impacts of Large (2.2 - 4.8 mm) Drops

The smallest drops for which a complete data set was taken in this region (2.7 mm) have a spectral density of $1.8 \times 10^{-8}$ $Pa^2/Hz$ at 10 kHz. The largest drops examined (4.6 mm) have a spectral density of $8.6 \times 10^{-6}$ $Pa^2/Hz$ at 10 kHz. A typical spectrum of

a 4.2 mm drop is shown in Figure 15 and was taken with a hydrophone depth of six cm. A summary of the spectral density at 10 kHz is given below in Table 2.
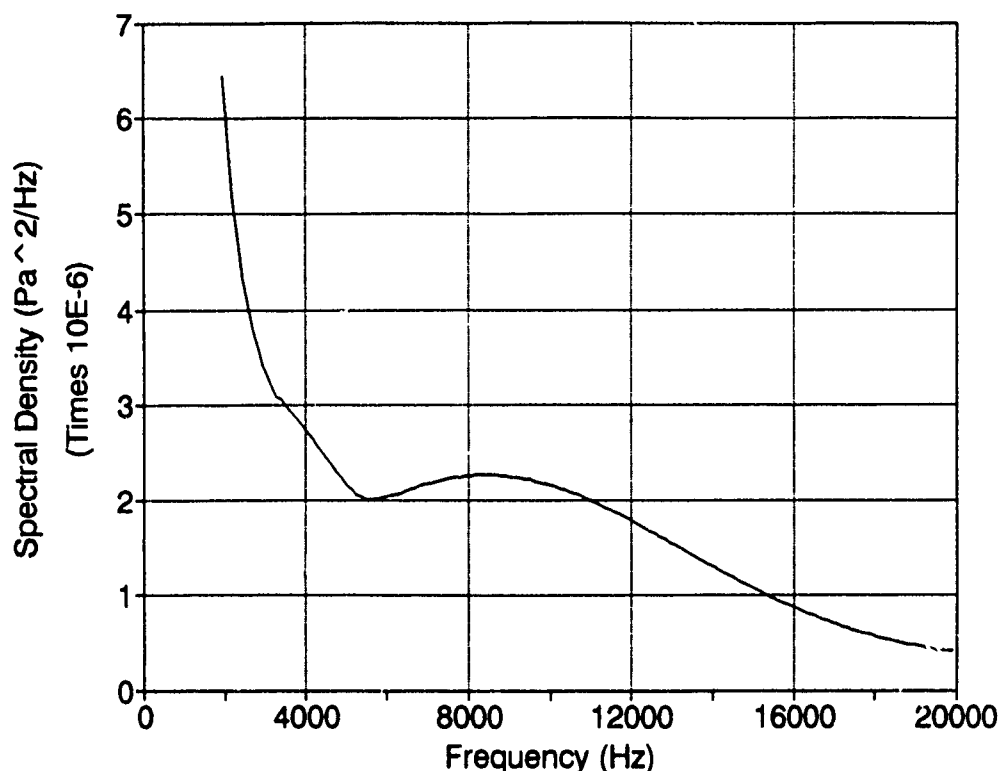


**Figure 15.** **Average Spectral Density of Impact of 4.2 mm Drop** (Sampled at 250 kHz; Record Length 256 $\mu$sec)

Because of the dynamics of the drop oscillations at impact, secondary peaks occur in the spectral density at about 25 kHz (unknown cause) and 90 kHz (internal reflections in the drop), as shown by Snyder's (1990) work. These are not considered in this analysis because they are small in magnitude and are outside the frequency range of interest in this study ( < 20 kHz).

Impacts from this range of drop size produce a comparatively large amount of acoustic energy per impact. However, relatively few of the largest drops occur in most natural rainfalls, and the overall magnitude of the contribution to the energy spectrum is approximately the same as that for the mid-sized drops. For example, using the 92 mm hr curve shown in Figure 3, 2705 mid-sized drops fall for each 21 drops of 4.6 mm diameter (calculations shown in Table 10). Assuming that the mid-size drops contribute

31

**Table 2.  IMPACT SPECTRAL DENSITY AT 10 KHZ**

| Drop Diameter (mm) | Magnitude $Pa^2/Hz$ |
|---|---|
| 2.7 | $1.8 \times 10^{-8}$ |
| 3.1 | $1.7 \times 10^{-7}$ |
| 3.4 | $3.6 \times 10^{-7}$ |
| 3.6 | $3.8 \times 10^{-7}$ |
| 4.0 | $2.2 \times 10^{-6}$ |
| 4.2 | $2.2 \times 10^{-6}$ |
| 4.6 | $8.6 \times 10^{-6}$ |

0.1 pJ per drop (Figure 16) and the 4.6 mm drop contribute 12 pJ per drop, 271 pJ of mid-size drop energy are radiated for each 252 pJ of energy radiated by the 4.6 mm drops.

A comparison of the sound energy radiated by the impact as a function of the impact kinetic energy is shown in Figure 16 and is summarized in Table 3. The drop kinetic energy was based on the known mass of the drop and its terminal velocity. According to Figure 16, approximately $10^{-9}$ of the drop's kinetic energy is converted into impact acoustic energy. This fraction of energy conversion is consistant with published literature (Kurgan, 1989;Medwin, et al., 1990).

**Table 3.  AVERAGE IMPACT ENERGY**

| Drop Diameter (mm) | Energy (pJ) |
|---|---|
| 1.0 | $0.01 \pm 0.002$ (Kurgan) |
| 2.7 | $0.66 \pm 0.19$ |
| 3.1 | $0.72 \pm 0.21$ |
| 3.4 | $0.90 \pm 0.26$ |
| 3.6 | $1.4 \pm 0.4$ |
| 4.0 | $5.5 \pm 1.6$ |
| 4.2 | $4.0 \pm 1.1$ |
| 4.6 | $12 \pm 3.5$ |
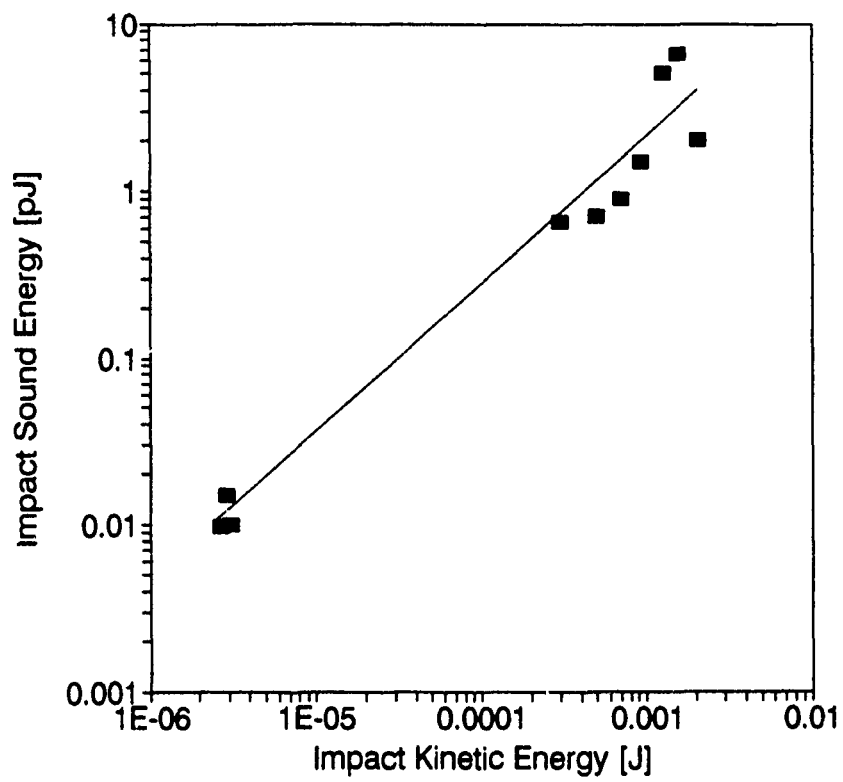
Figure 16.    Average Impact Sound Energy vs. Drop Kinetic Energy

## D. BUBBLE ENERGY

### 1. Type I Bubble Spectral Density and Peak Pressure

The sound radiated by Type I bubbles has been extensively measured (Kurgan, 1989; Medwin, et. al., 1990; Pumphrey and Elmore, 1990). It is known that Type I bubbles are produced by small drops falling at terminal velocity and by larger drops impacting at lower velocities (Regular entrainment/Large Bubble regions of Figure 8). The acoustic energy for small, terminal velocity bubbles is contained in a very narrow bandwidth centered at about 15 kHz. Peak sound pressure for this size is 0.4 - 0.5 Pa (Kurgan, 1989), which agrees well with the predictions of analytical models (Longuet-Higgins, 1990). The total energy for this size is about 1 - 3 pJ (Kurgan, 1989). A typical spectral density for a Type I bubble is shown in Figure 17 and was acquired with the setup described in Section II.A.7.
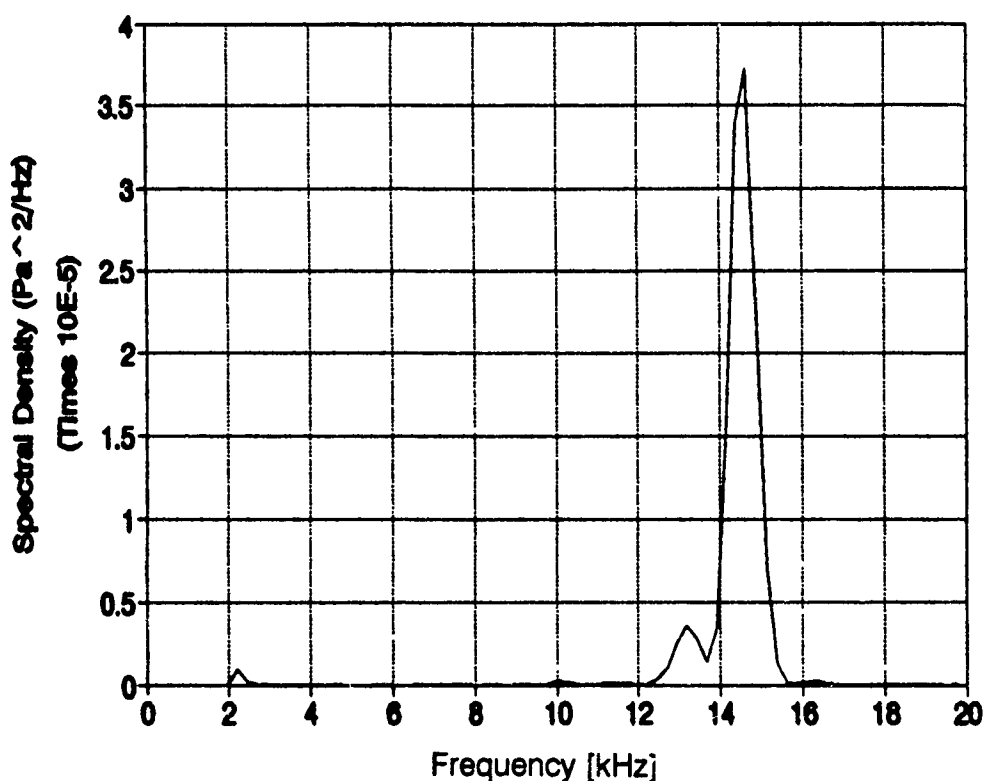


**Figure 17.** Spectral Density of a Type I Bubble (Sample Frequency 250 kHz; Frequency Resolution 122 Hz)

## 2. Type II Bubble Average Spectral Densities at 1 m on Axis (20 C)

Type II bubbles from terminal velocity drops have been researched only recently (Snyder, 1990), and little was previously known about the energy of this type of bubble. Although this region has been labeled "irregular entrainment" (Pumphrey, et. al., 1989), the terminal velocity portion of this region has been shown to produce bubbles a predictable percentage of the time (Snyder, 1990), as shown in Figure 18. The percentage of bubble production varies from 0 % at 2.2 mm diameter to a maximum of 62 % at 3.7 mm. The decrease in percentage of bubbles generated by drop sizes larger than 4.2 mm suggests that beyond this size, the "excess" kinetic energy begins to disrupt the delicate balance of the mechanism that causes the bubble to form.
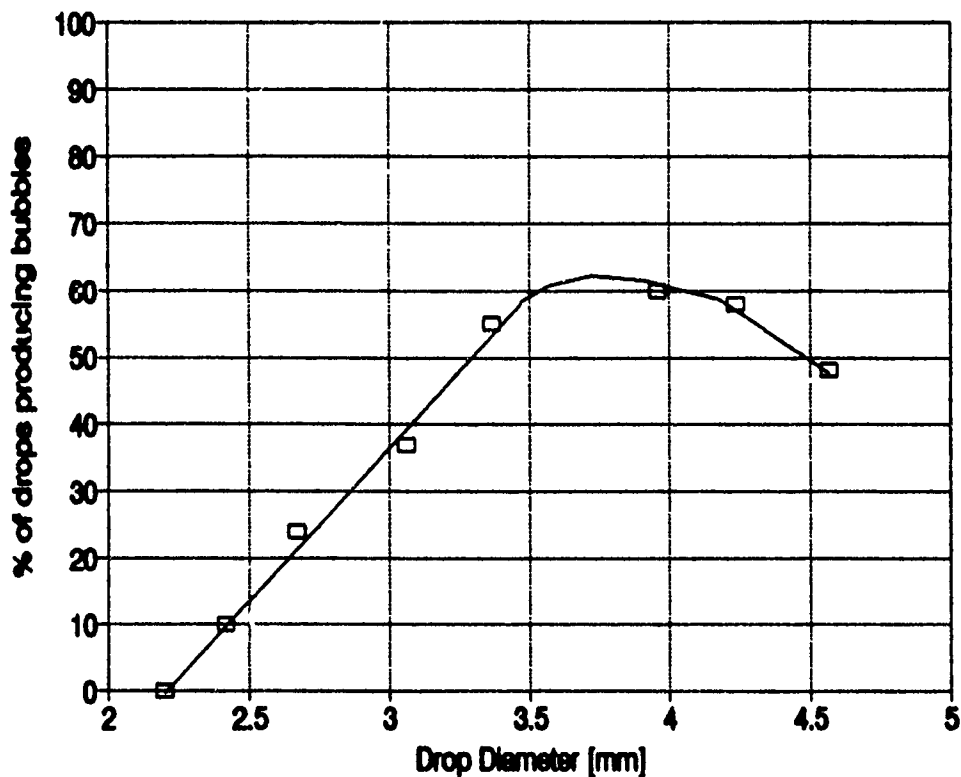


Figure 18.    Bubble Creation Percentage (% of Drops with Bubbles vs. Drop Diameter)

The average spectral energy radiated by Type II bubbles generally increases with drop size. The smaller drop sizes, 2.7 mm - 3.7 mm, each show a dominant peak of the

35

bubble radiation. The average spectral density of the bubbles from 3.1 mm drops is shown in Figure 19. The spectrum of each drop size is relatively broad and secondary peaks ave evident in several drop diameters. This is evidence that very energetic bubbles can occur at frequencies other than that of the peak.
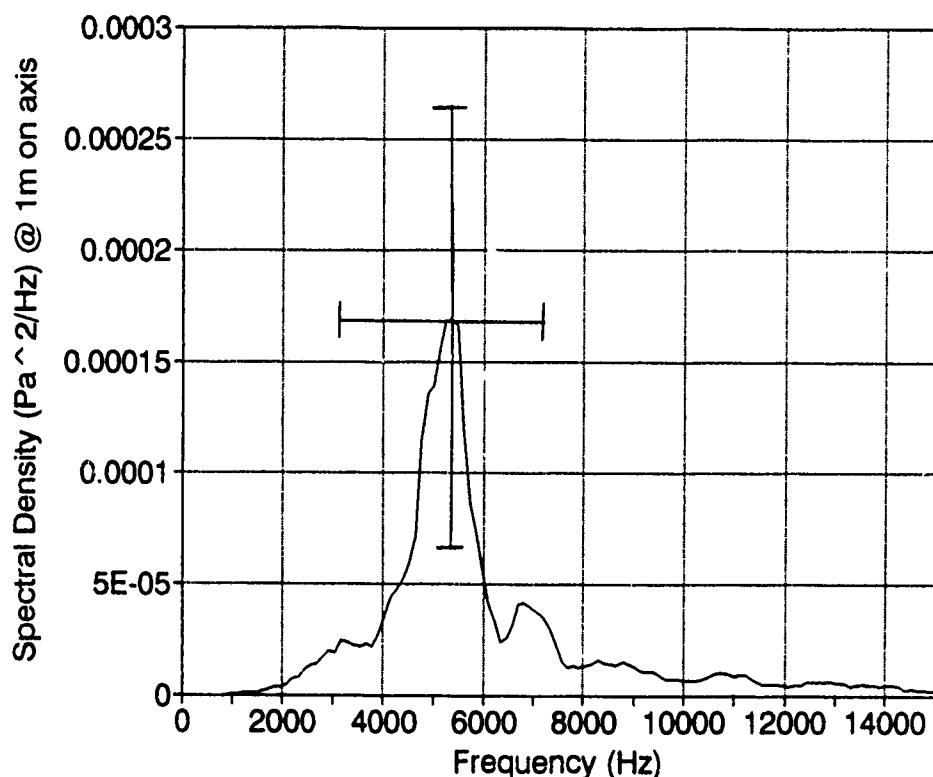


**Figure 19.** **Average Spectral Density of Bubble From 3.1 mm Drops**

The estimate of the standard deviation of spectral density at any given frequency can be quite large. This is due to the combination of deviation in frequency and amplitude of the dominant bubble. The standard deviation observed at sea will be much less than that obtained the laboratory due to the larger sample space. For example, in the case of the 92 mm/hr rainfall shown in Chapter I, approximately 18 drops with a diameter of 4.6 $\pm$0.2 mm fall in each $m^2$ per second. For a typical surface area of 250 $m^2$ that a hydrophone may hear, a 30 second sample (also typical) will yield approximately 135,000 drops! This is enough to reduce the standard deviation seen in the laboratory by several orders of magnitude. The standard deviations of the laboratory work are presented here both for the dominant bubble frequency and for the magnitude of the

spectral density. This is the best way to gain appreciation for the way in which the dominant bubble varies.

The 3.4 mm drops produced bubbles with average dual peak spectral densities of $1.3\pm0.7 \times 10^{-4}$ Pa²/Hz and $1.2\pm0.5 \times 10^{-4}$ Pa²/Hz at frequencies of 5.0 kHz and 2.3 kHz (Figure 20). The 5.0 kHz peak is caused by primary bubbles. The peak at 2.3 kHz is caused by wobbles and the smaller peak at 8.2 kHz is caused by secondary bubbles. This is the only drop diameter observed which contained significant secondary peaks (within 3 dB of the dominant bubble peak).
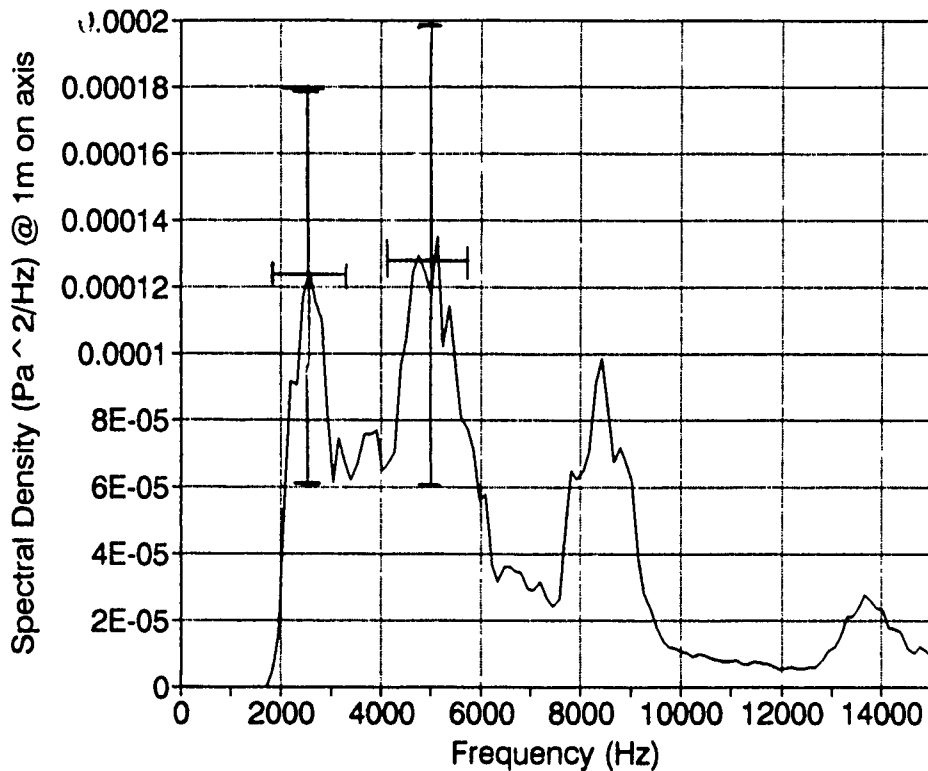


Figure 20.    Average Spectral Density of Bubble From 3.4 mm Drops

The 4.2 mm drops produced bubbles with an average peak spectral density of $1.5\pm0.9 \times 10^{-2}$ Pa²/Hz at 1.9 kHz. A single, slightly broader peak is visible. No evidence of secondary bubbles is present.

The peak spectral density for the largest drop (4.6 mm) is $1.2\pm0.7 \times 10^{-2}$ Pa²/Hz and occurs at 1.8 kHz (Figure 21). A single peak is present, and evidence of secondary

bubbles (discussed later) at 8 kHz is evident. The average peak spectral densities for various drop sizes are summarized in Table 4 below.
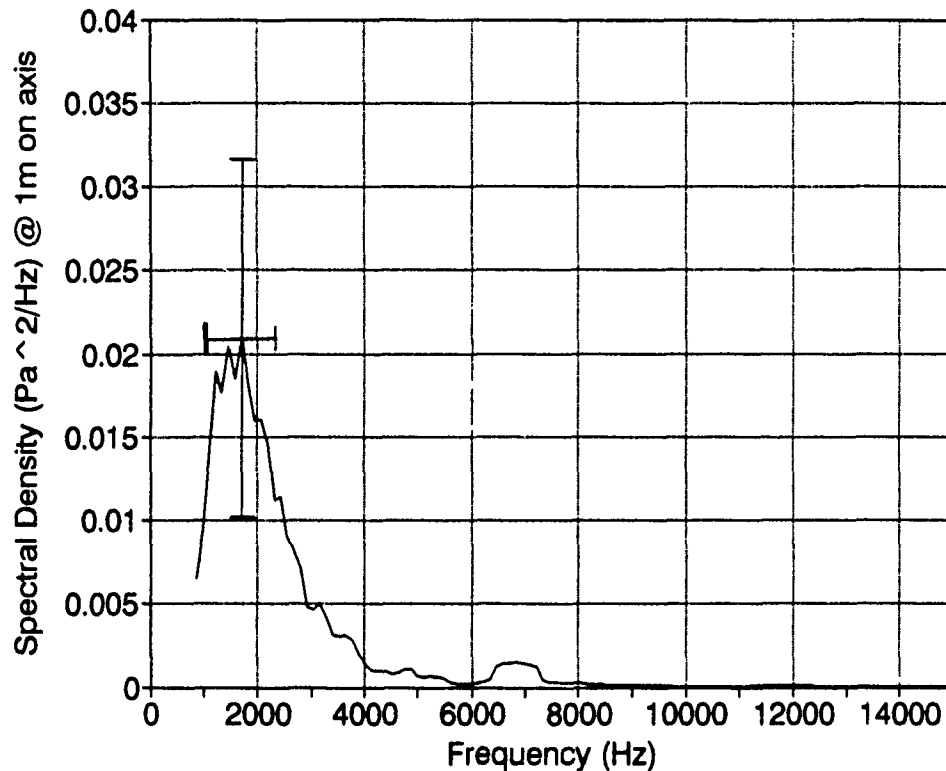


**Figure 21.** **Average Spectral Density of Bubble From 4.6 mm Drops**

The frequency at which the spectral density peaks is directly related to drop size. This is similar to the work done by Snyder, which related the frequency of the dominant bubble to drop diameter (Snyder, 1990). The exact relation of frequency to drop size is different in this work due to a different method of selecting the frequency at which the peak occurs. The work by Snyder selected the dominant bubble frequency from each individual bubble spectrum and then took the average of the frequencies for each drop size. In contrast, this work averaged all of the spectral densities for a given drop size and then determined the peak of the average. The previous method retains only one peak frequency per spectrum and ignores the rest. The current method keeps all of the details of the spectrum but is more susceptible to a single spectrum dominating the entire average if the magnitude is much larger. Both are valid methods of obtaining the fre-

38

**Table 4. TYPE II BUBBLE AVERAGE PEAK SPECTRAL DENSITY SUMMARY**

| Drop Diameter (mm) | Frequency (Hz) | Peak Spectral Density (on axis at 1 m) Magnitude $Pa^2/Hz$ |
|---|---|---|
| 2.7 | 8500 $\pm$1200 | $6.0\pm3.3 \times 10^{-4}$ |
| 3.1 | 5200 $\pm$2000 | $1.8\pm1.1 \times 10^{-3}$ |
| 3.4 | 5000 $\pm$1200 | $1.3\pm0.7 \times 10^{-4}$ |
| 3.6 | 4200 $\pm$750 | $6.3\pm6.0 \times 10^{-3}$ |
| 4.0 | 2400 $\pm$900 | $9.0\pm7.2 \times 10^{-3}$ |
| 4.2 | 1900 $\pm$950 | $1.5\pm0.9 \times 10^{-2}$ |
| 4.6 | 1800 $\pm$900 | $2.2\pm1.2 \times 10^{-2}$ |

quency at which a given relation peaks, but the results connotate different meanings. The results of both methods are shown in Figure 22.
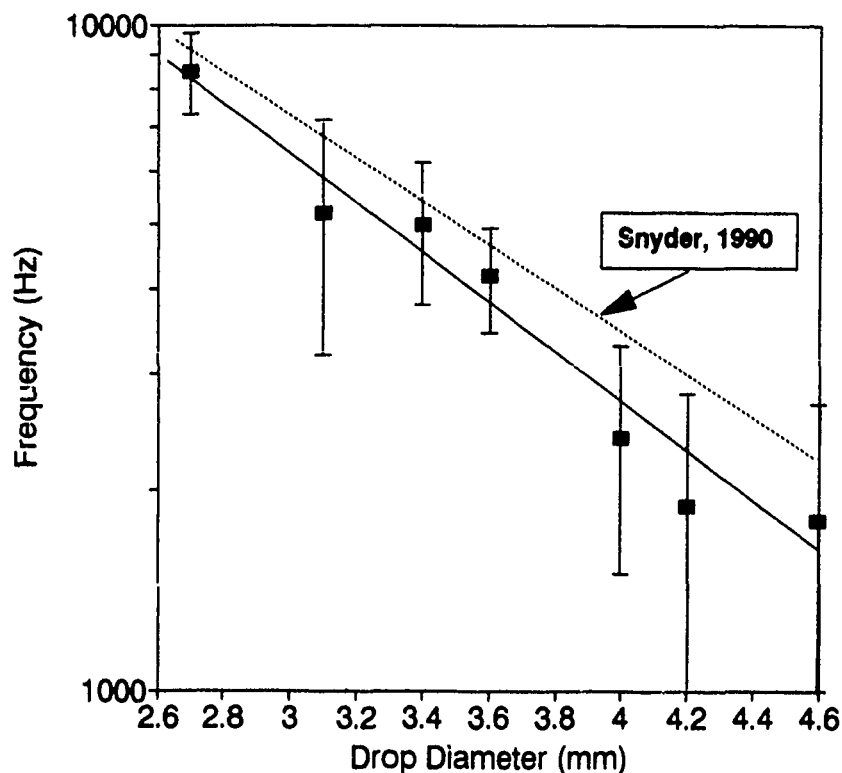
**Figure 22.  Frequency of the Peak Spectral Density vs. Drop Diameter**

## E.  ENERGY DUE TO SECONDARY EFFECTS

### 1.  Secondary Bubble Energy

In approximately 12% of the bubbles analyzed, a second, higher frequency bubble was noted as well.  This bubble could occur before, during or after the dominant bubble.  The sound radiation from this secondary bubble was always smaller in peak magnitude and higher in frequency.  Higher frequency bubbles have a higher damping rate (Devin, 1959).  Based on these observed characteristics, secondary bubbles have lower energy than dominant bubbles.  The secondary bubble was mentioned as a possible source of some of the sound produced by rainfall in recent field work (Tan, 1990). It should not be considered as a primary source of sound, as its energy is between 7 to 27% of the energy in the dominant bubble.  A summary of secondary bubble production is given in Table 5.

**Table 5.   SUMMARY OF NUMBERS OF SECONDARY BUBBLES**

| Drop Diameter (mm) | Drops Producing Dominant Bubbles | Drops producing Secondary Bubbles and Dominant Bubbles | Percent |
|---|---|---|---|
| 2.7 | 29 | 2 | 7% |
| 3.1 | 36 | 1 | 3% |
| 3.4 | 33 | 7 | 21% |
| 3.7 | 14 | 2 | 14% |
| 4.0 | 28 | 4 | 14% |
| 4.2 | 29 | 5 | 17% |
| 4.6 | 30 | 2 | 7% |

## 2.   Wobble Energy

The most unique secondary effect investigated was the "wobble," which derives its name from its appearance in the time domain (Figure 13). It starts and stops abruptly and can occur before or during the dominant bubble. Its frequency is most often below 3 kHz and, because it is generally weaker than the radiation from the dominant bubble, it does not affect the overall spectrum, except for the case of 3.4 mm drops. For the 3.4 mm drop, the peak spectral density level due to the wobble is equal to that due to the dominant bubble, the result of which is two peaks (Figure 20).

The wobble is most likely caused by the spatial variability of the turbulent jet as it protrudes though the crater and moves into the ambient water. It may be an oscillation of the crater itself caused by the jet stream acting as a piston in driving the crater into oscillation. High speed photographs do show variability in the width of the jet. It was not possible, however, to directly determine the frequency of the oscillations using the ripples on the jet because the film speed limit was approximately 400 frames per second. This is equivalent to sampling a 3 kHz oscillation at 400 Hz and consequently violates the Nyquist sampling criterion.

The percentage of drops which form wobbles is directly proportional to the drop size (shown in Table 6). This means that the wobble production rate is directly proportional to the incident kinetic energy. A higher energy impact would more likely produce a more turbulent jet than a lower energy impact. This jet, in turn, could be more likely to cause the crater surface to oscillate and radiate sound.

41

Table 6.  WOBBLE FORMATION SUMMARY

| Drop Diameter (mm) | Drops Producing Dominant Bubbles | Drops Producing Wobbles and Dominant Bubbles | Percent |
|---|---|---|---|
| 2.7 | 29 | 0 | 0% |
| 3.1 | 36 | 8 | 8% |
| 3.4 | 33 | 5 | 15% |
| 3.7 | 14 | 4 | 29% |
| 4.0 | 28 | 11 | 39% |
| 4.2 | 29 | 10 | 34% |
| 4.6 | 30 | 15 | 50% |

The wobble spectral peak is generally narrower than that of a bubble for the same drop size (Figure 23), which means that the energy is confined to a smaller frequency range. This agrees well with the time domain signal in which the wobble appears as a gated sinusoid with a nearly constant period. The frequency at which the wobble radiates also appears to be more uniform for a given drop size, as shown by the smaller standard deviations in Table 7.

Table 7.  DOMINANT BUBBLE FREQUENCY VS. WOBBLE FREQUENCY

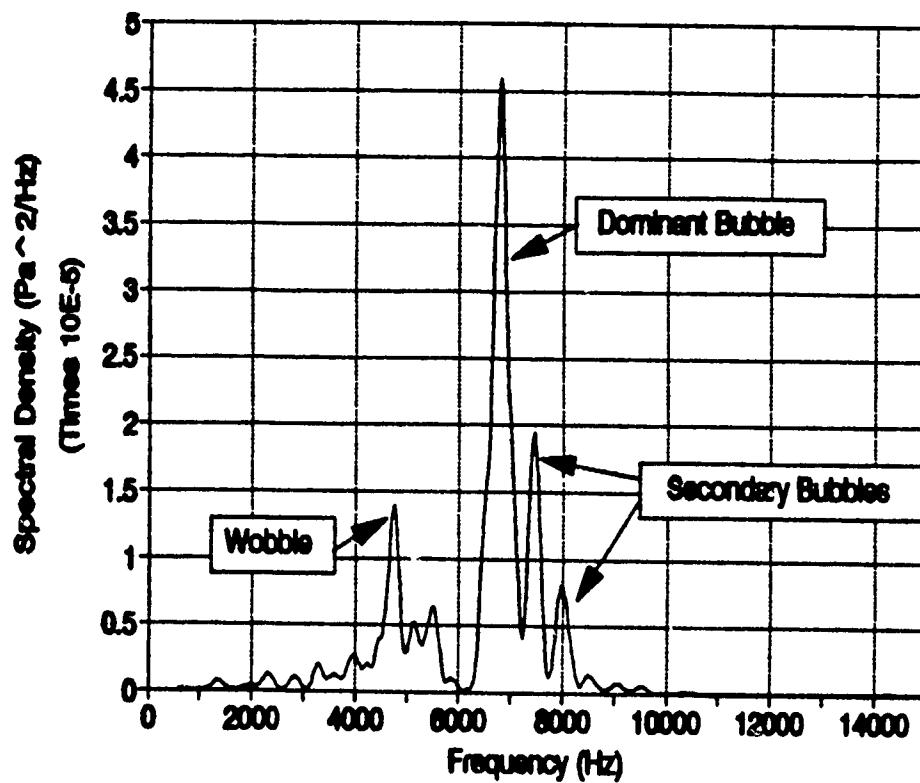| Drop Size (mm) | Wobbles | | | Dominant Bubbles | | |
|---|---|---|---|---|---|---|
| | No. | Frequency (kHz) | Standard Deviation (kHz) | No. | Frequency (kHz) | Standard Deviation (kHz) |
| 4.0 | 11 | 2609 | 786 | 28 | 4023 | 1669 |
| 4.2 | 10 | 1695 | 402 | 29 | 3676 | 1744 |
| 4.6 | 15 | 1946 | 642 | 30 | 2850 | 1032 |

Figure 23.  Spectral Density of a 4.2 mm Drop Showing Different Contributions to the Radiated Energy

## F.  TOTAL ENERGY PER RAINDROP AT ROOM TEMPERATURE (20 °C)

The amount of energy produced by an *average* large raindrop is a combination of the impact and the dominant bubble energy, as well as "wobbles" and secondary bubble radiation.  The calculation of energy per average drop must account for the fact that bubbles are created in only a given percentage of time whereas impacts are present in all drops.  Overall, the energy radiated from dominant bubbles (and secondary bubbles as well as the wobble when they occur) is far greater than that radiated by the impact.

The axial peak spectral density per raindrop varies from $3.4 \pm 1.9 \times 10^{-5}$ Pa$^2$/Hz for the 2.7 mm drop to $3.2 \pm 1.8 \times 10^{-3}$ Pa$^2$/Hz for the 4.6 mm drop.  A summary of peak spectral levels is given in Table 8.

**Table 8.  PEAK SPECTRAL DENSITY PER RAINDROP SUMMARY**

| Drop Size [mm] | Frequency [Hz] | Peak Spectral Density [$Pa^2/Hz$] |
|:---:|:---:|:---:|
| 2.7 | 8500 ±1200 | $3.4 \pm 1.9 \times 10^{-5}$ |
| 3.1 | 5200 ±2000 | $2.8 \pm 1.5 \times 10^{-4}$ |
| 3.4 | 5000 ±1200 | $1.2 \pm 0.7 \times 10^{-4}$ |
| 3.6 | 4200 ±750 | $1.4 \pm 1.3 \times 10^{-3}$ |
| 4.0 | 2400 ±900 | $1.6 \pm 1.3 \times 10^{-3}$ |
| 4.2 | 1900 ±950 | $4.7 \pm 2.8 \times 10^{-3}$ |
| 4.6 | 1800 ±900 | $3.2 \pm 1.8 \times 10^{-3}$ |

The magnitude of peak spectral density for different drop diameters varies by an enormous amount, with two decade of difference between the spectral density level peak of the 2.7 mm drop as compared to that of the 4.6 mm drop.  It may seem as if the sound generated by rainfall would be completely dominated by the largest of drops.  However, Nature strikes a balance by producing very few large drops and thereby enables all drop diameters to contribute meaningfully to the overall rainfall spectrum.

The average axial spectral density levels (bubble and impact) are shown in Figure 24 through Figure 30.  The plots do take into account that a bubble is created only a given percentage of the time, whereas the impact always radiates sound.  Also plotted are the impact spectral density levels for comparison.
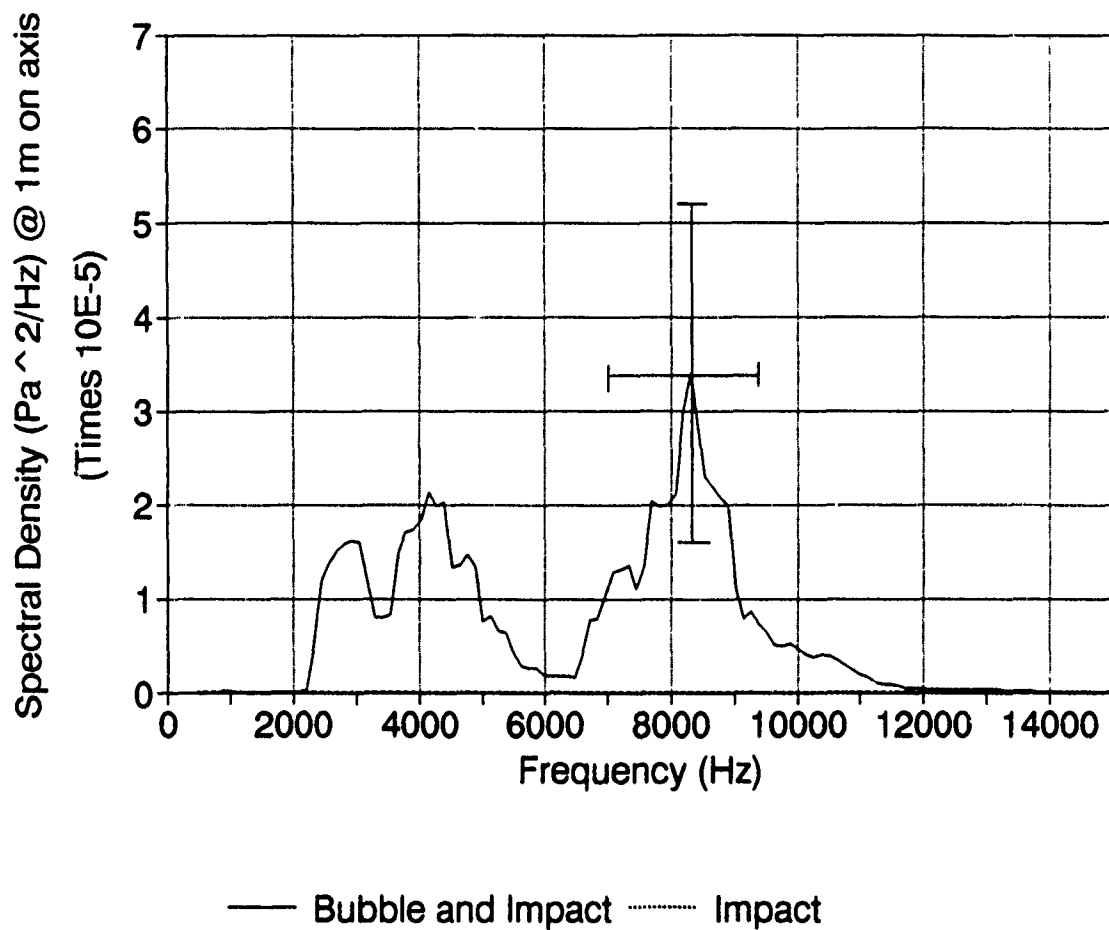
Figure 24.    Average Axial Spectral Density per 2.7 mm Drop
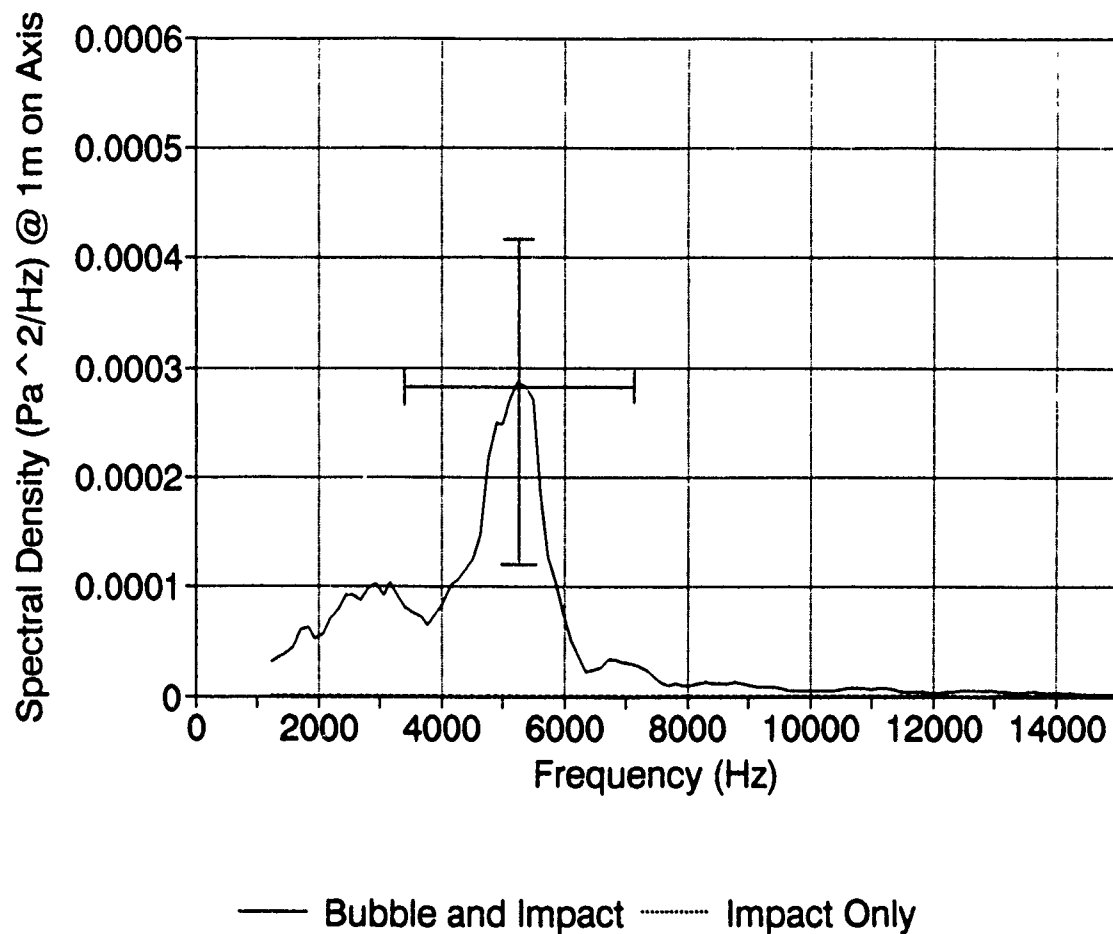
Figure 25. Average Axial Spectral Density per 3.1 mm Drop
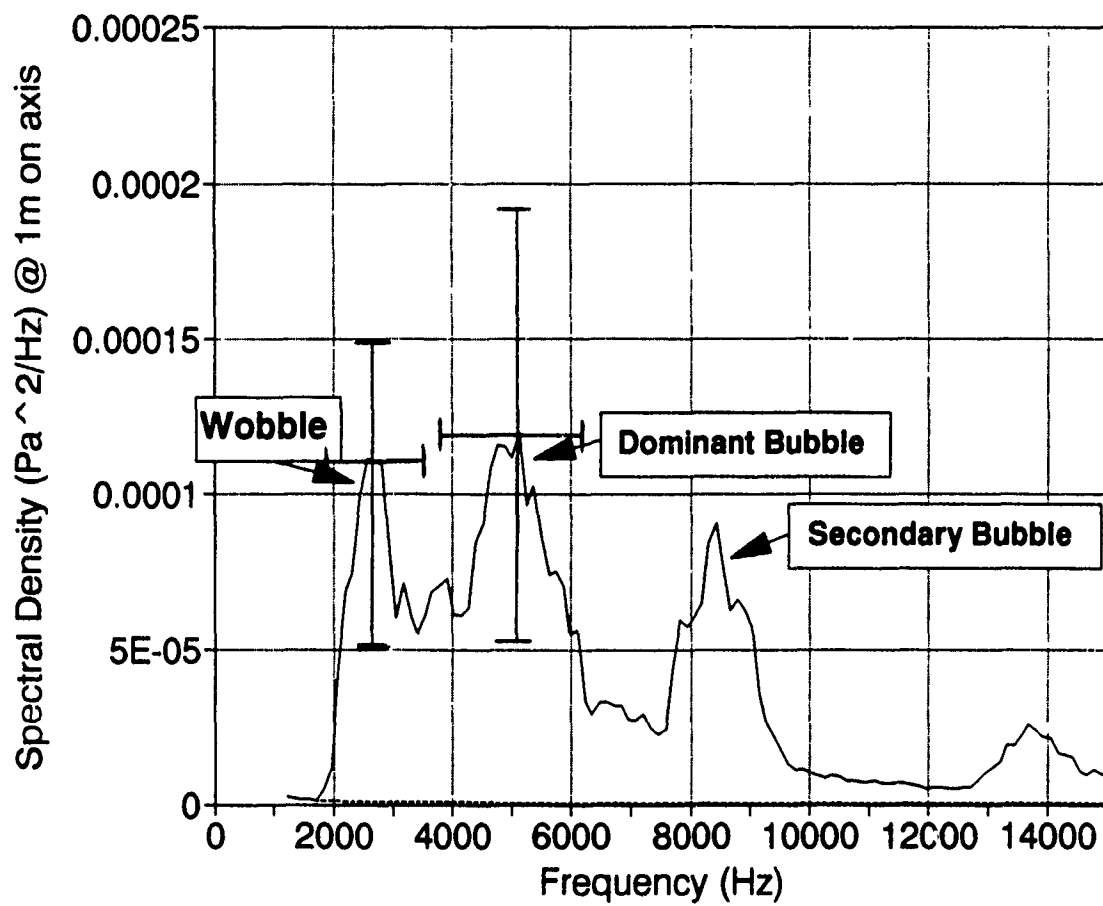
Figure 26.    Average Axial Spectral Density per 3.4 mm Drop
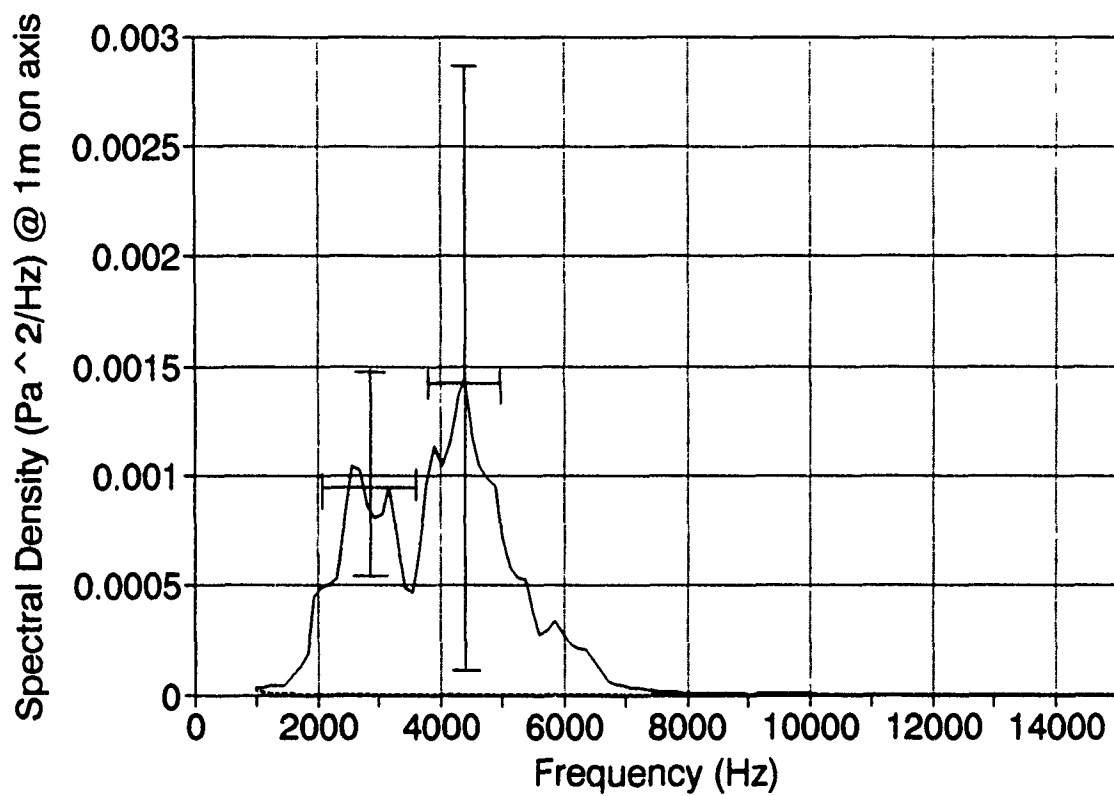
Figure 27.   Average Axial Spectral Density per 3.6 mm Drop
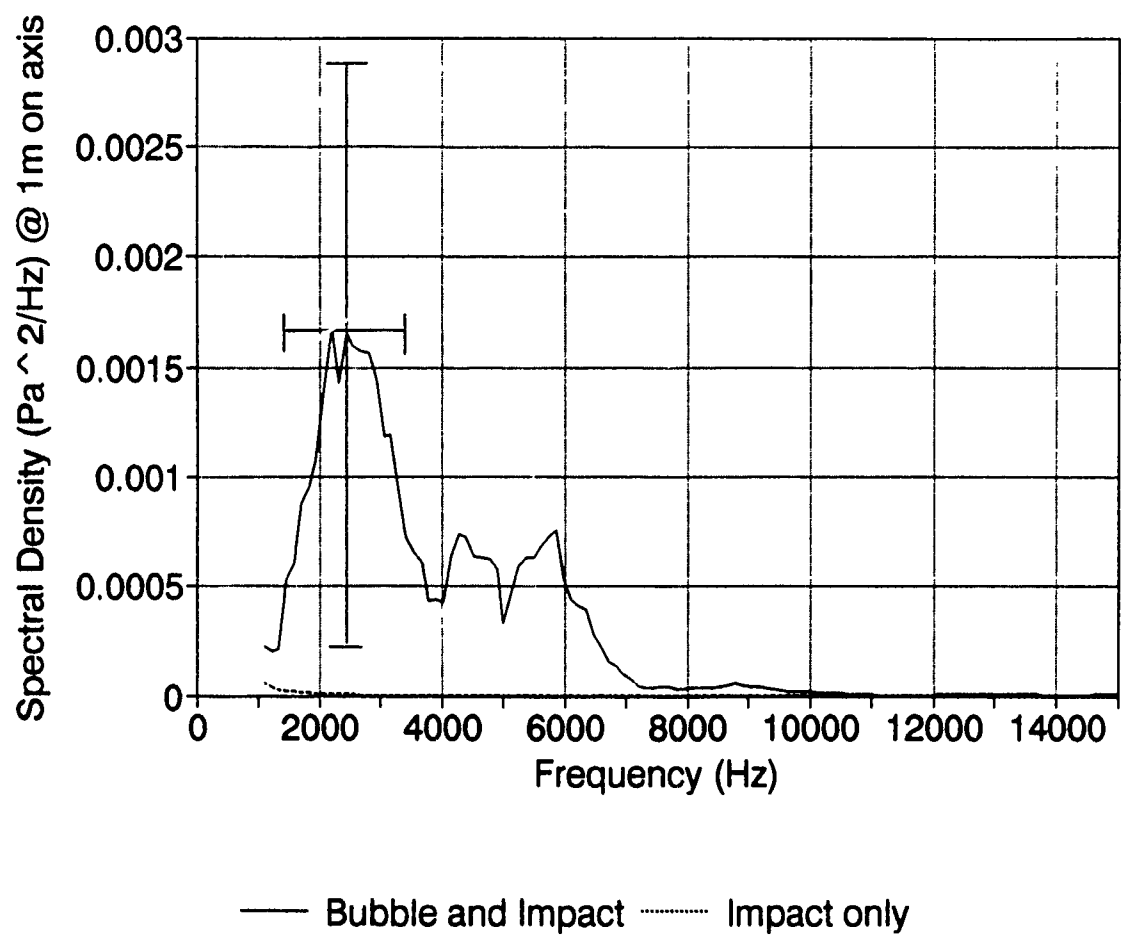
Figure 28. Average Axial Spectral Density per 4.0 mm Drop

49
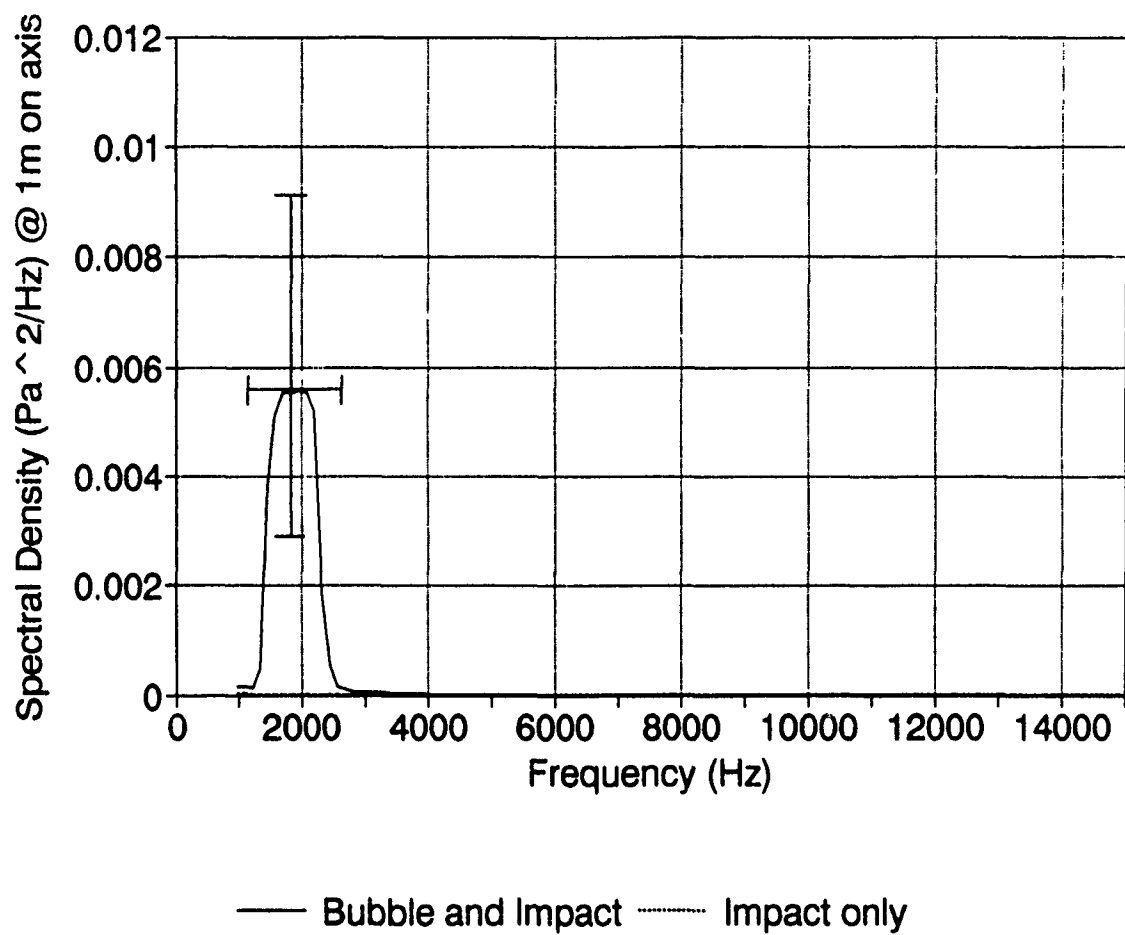
Figure 29.    Average Axial Spectral Density per 4.2 mm Drop
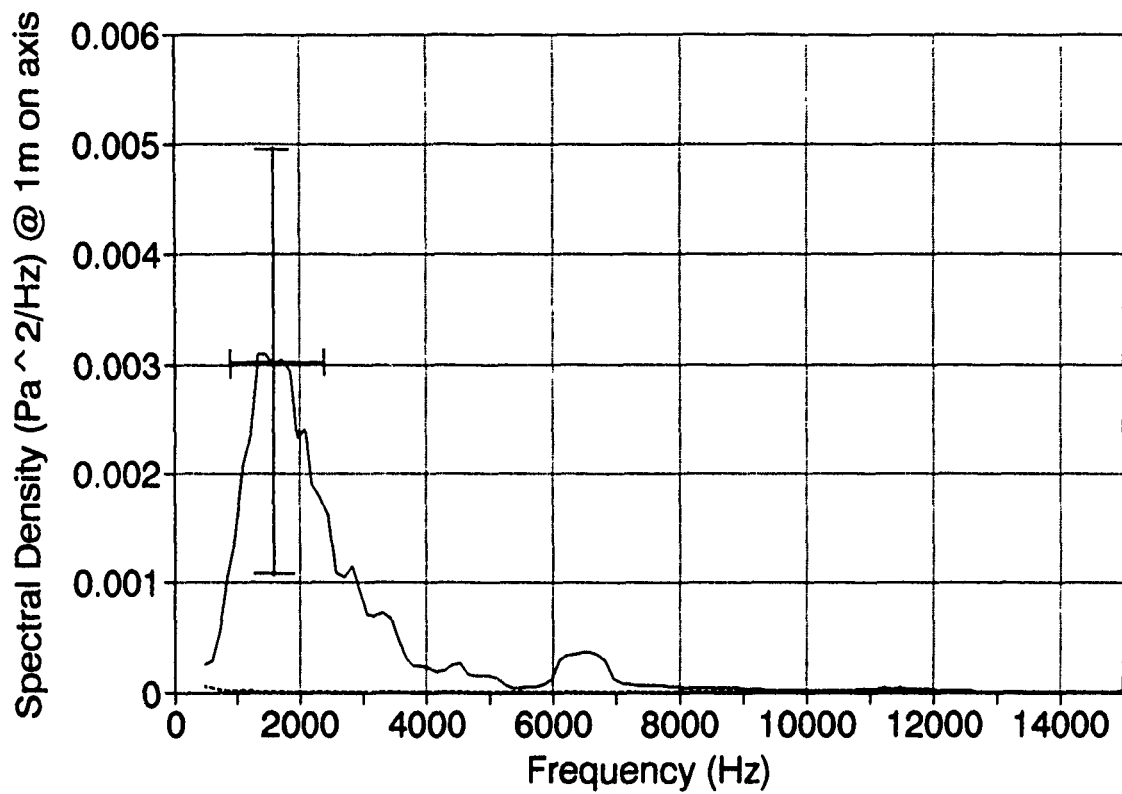
Figure 30.    Average Axial Spectral Density per 4.6 mm Drop

The integral of the average axial spectral density over frequency is proportional to the energy radiated by the raindrop. Using Eqn. 11, with R = 1m and *Time* = .8.2 ms, the average energy per raindrop (20°C) for diameters between 1.0 mm - 4.6 mm is given in Table 9:

Table 9.  AVERAGE ACOUSTIC ENERGY PER RAINDROP (20 C)

| Drop Diameter (mm) | Energy (pJ) |
|:---:|:---:|
| 1.0 | 1.5 (Kurgan, 1989) |
| 2.7 | 12 ±4 |
| 3.1 | 69 ±37 |
| 3.4 | 69 ±40 |
| 3.6 | 320 ±280 |
| 4.0 | 440 ±330 |
| 4.2 | 470 ±290 |
| 4.6 | 559 ±260 |

# VI. COMPARISON OF CALCULATED AND MEASURED RAINFALL SPECTRA

## A. METHOD OF CALCULATION

### 1. Background

It is a natural extension, given the results of the previous chapter, to calculate the rainfall spectrum for a given drop size distribution (DSD) and compare the calculated results with *in situ* measurements. Unfortunately, the only published data which contains both drop size distribution and rainfall spectrum (RS[f]) states only the number of drops which struck the distrometer and does not include information necessary to extract the number of drops falling per $m^2$ per second (Scrimger, et al., 1987). Future experiments planned by this laboratory will include simultaneous measurements of drop size distribution and underwater spectrum levels for light to heavy rainfall.

We can, however, calculate a rainfall spectrum due to a given drop size distribution and compare the results to a rainfall spectrum (with the same rainfall rate) obtained elsewhere. In this manner, it is possible to match only **total rainfall rate** and not the drop size distribution. This, of course, will cause the calculated spectrum to suffer an unknown (but bounded) error.

### 2. Comparison With a Known Hydrophone Geometry

Many underwater spectrum levels were available from J. Nystuen's rainfall research at the Ocean Test Platform (OTP) in the Gulf of Mexico, as well as published work (Tan, 1990; McGlothin, 1991). The location of the OTP is shown in Figure 31 and the hydrophone geometry is given in Figure 32. For the frequency range of interest, the hydrophone had an upward looking 3 dB beam of 30° and was located at a depth of 15 m. The beam was therefore able to "hear" a circular surface area with a radius of 7.5 m. The diffraction effects of the hydrophone mounting are being studied.
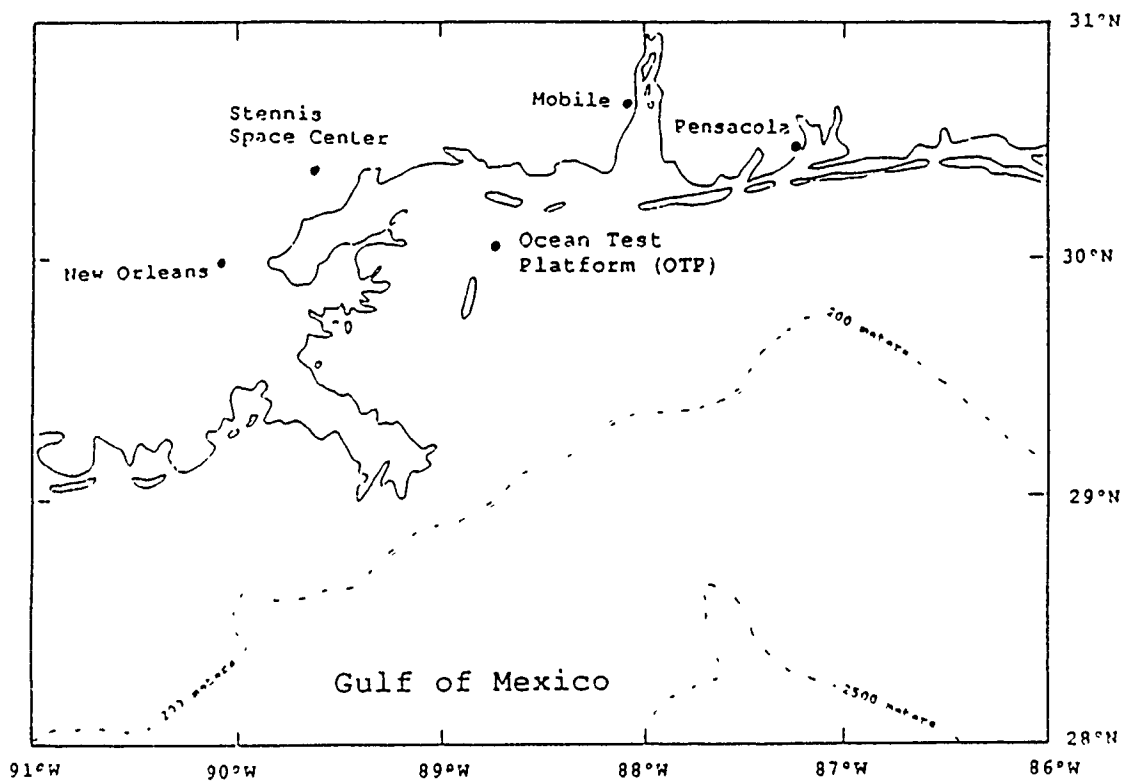
Figure 31.  Ocean Test Platform Location

1. OPTICAL RAIN GAUGE
2. WIND SPEED SENSOR
3. RAIN ACCUMULATION SENSOR
4. DIRECTIONAL WAVE MEASURING SYSTEM
5. DAT RECORDER, MODEL 6 DATA LOGGER
6. HYDROPHONE CABLE
7. HYDROPHONE
8. HYDROPHONE SUPPORT FIXTURE
9. ANCHOR CHAIN (3-POINT MOOR)
10.6000 LBS ANCHOR
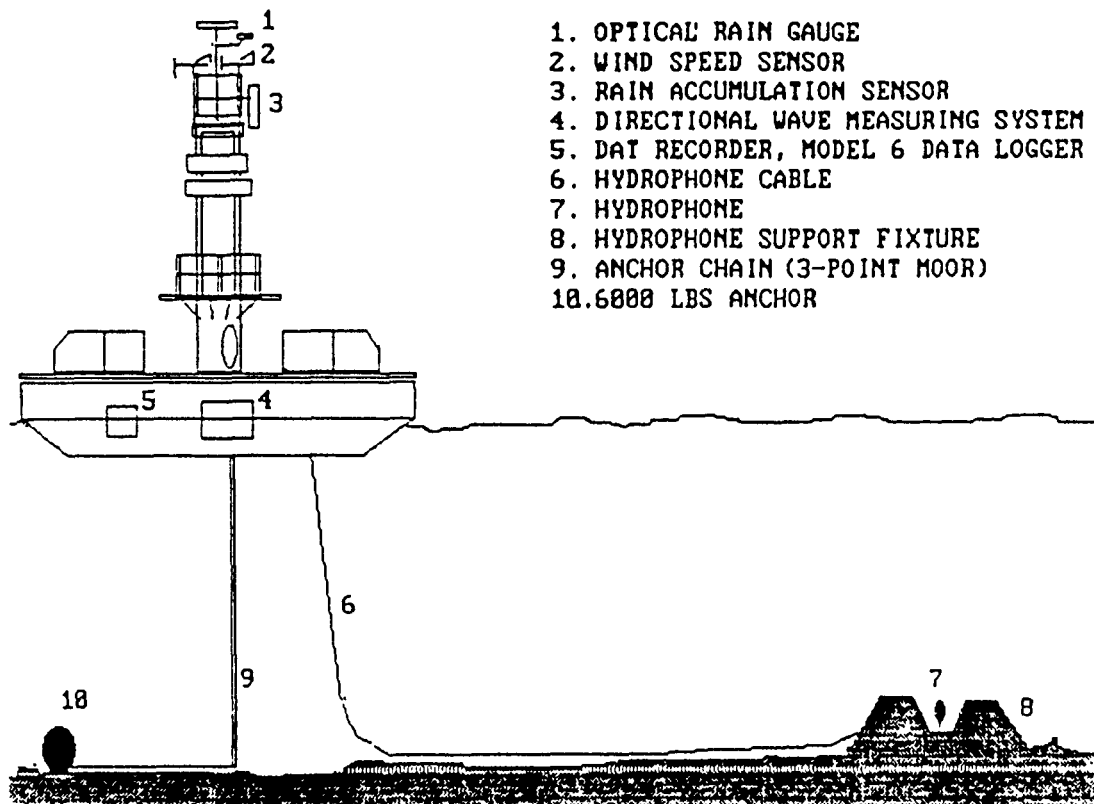
**Figure 32.    Ocean Test Platform Hydrophone Geometry**

The calculated rainfall spectrum must account for the range to the hydrophone being greater at the edge of the surface area than directly overhead and the cos $\theta$ dropoff for dipole radiation. Both of these effects tend to decrease the intensity at the edge of the surface area and can be accounted for by the integration of pressure over small concentric rings (Figure 33).

55
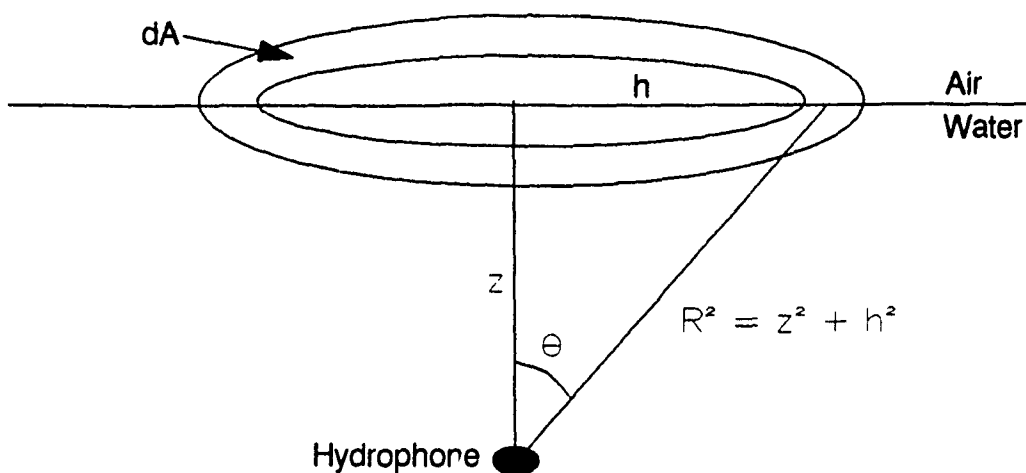
**Figure 33.**   **Concentric Ring Integration.**

For a hydrophone with 3 dB beamwidth $\psi$ (for a point hydrophone or omnidirectional hydrophone $\psi = 90°$) the rainfall spectrum (RS(f)) is calculated by:

$$RS(f) = \sum_{D} \int_{0}^{h} \left( DRD(D) \times SD(f,D) \times \cos^2\theta \times \frac{[1]^2}{R^2} \times 2\pi\, h'\, dh' \right) \times T_s \qquad (14)$$

where DRD(D) is the drop rate distribution of the diameter indexed in the summation in *Drops/m² s*, SD(f,D) is the spectral density of the drop diameter indexed in the summation in *Pa²/Hz Drop*, $\theta$ varies from 0 to $\psi$ as $h'$ varies from 0 to h. Using the substitutions $z = R\cos\theta$, $h = R\sin\theta$ and $dh = z\sec^2\theta\, d\theta$, this reduces to:

$$RS(f) = \sum_{D} \int_{0}^{\psi} (DRD(D) \, SD(f,D) \, 2\pi \, \cos\theta \, \sin\theta \, d\theta) \, T_s \qquad (15)$$

Evaluation of the integral yields the result:

$$RS(f) = \sum_{D} \pi \times DRD(D) \times SD(f,D) \times \sin^2\psi \times T_s \qquad (16)$$

To convert RS(f) to a spectrum level RSL(F) (dB):

$$RSL(f) = 10 \log RS(f) \qquad (17)$$

## B. COMPARISON WITH OCEAN SPECTRUM LEVELS

The drop size distributions used for these comparisons are shown in Figure 3 and were obtained in 1982 at Clinton Lake, IL (Courtesy J. Nystuen). They are similar to the Marshall-Palmer distribution (Marshall and Palmer, 1948). The rainfall spectrum levels were obtained in 1990 at the OTP using an ITC Model 3001 hydrophone.

The drop rate for each diameter (Table 10) is calculated by multiplying the ordinate of Figure 3 by the increment of drop diameter and the terminal velocity of the drop. For example, using the curve of 92 mm/hr total rainfall rate, we desire to know how many 4.0 mm drops fall on each $m^2$ per second. Using Table 10, the increment of drop diameter is 0.3 mm ($\pm$0.15 mm). The terminal velocity for a 4.0 mm drop is 9.1 m/s (Snyder, 1990). The rainfall rate for 4.0 drops is therefore:

$$DRD(4.0\pm0.15mm) = 15\frac{drops}{m^3\,mm} \times 0.3mm \times 9.1m/s = 40.9\frac{drops}{m^2\,s} \approx 41\frac{drops}{m^2\,s} \quad (18)$$

It is preferable to calculate the rainfall spectra for several drop size distributions to ensure that the results are within reasonable tolerance to those found in natural rain. The result of this exercise (Figure 34), shows the calculated rainfall spectrum levels for 12 mm/hr, 52 mm/hr and 92 mm/hr rainfall rates and contains only the contributions due to Type II drops. The spectral density levels range from 57 to 95 dB re $1\mu Pa^2/Hz$ over the frequency range of interest, which is similar to the spectral densities reported in the literature (Tan, 1990; Scrimger, 1987). The separation between the 92 mm/hr and the 12 mm/hr curves is approximately 7 - 12 dB over the entire frequency range. The 52 mm/hr curve differs from the 92 mm hr curve by about 2 - 5 dB over the same range.

Table 10. DROP SIZE DISTRIBUTIONS USED IN RSL CALCULATIONS

| | 92 mm/hr | 52 mm/hr | 12 mm/hr |
|---|---|---|---|
| Drop Diameter, mm | Drops/$m^2s$ | Drops/$m^2s$ | Drops/$m^2s$ |
| 0.8 - 1.1 | 1278 | 450 | 621 |
| 1.1 - 2.4 | 2705 | 1364 | 1081 |
| 2.4 - 2.9 | 412 | 436 | 47 |
| 2.9 - 3.3 | 193 | 120 | 7.2 |
| 3.3 - 3.5 | 75 | 60 | 2.5 |
| 3.5 - 3.8 | 60 | 40 | 1 |
| 3.8 - 4.1 | 41 | 27 | None |
| 4.1 - 4.4 | 28 | 17 | None |
| 4.4 - 4.8 | 21 | 9 | None |

These differences are similar to those shown in Tan (1990). The results of the calculated rainfall spectrum levels are quite similar to those found in natural rainfall, and a more thorough comparison is desirable.
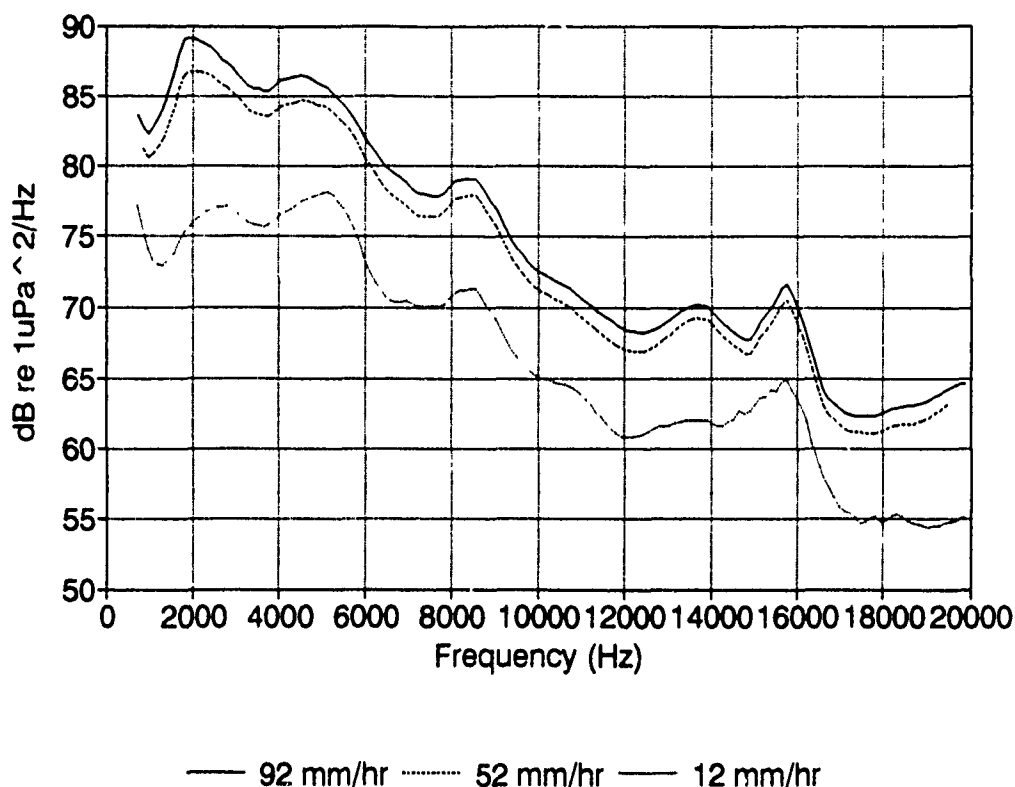
Figure 34. Calculated RSL for Various Rainfall Rates

Unfortunately, no ocean rainfall spectrum levels are available for the same rainfall rates considered above. Data is available, however, for 100 mm/hr and 15 mm/hr rainfall rates taken at OTP in the Gulf of Mexico. It is assumed for this prediction that the 92 mm/hr calculated RS(f) can be linearly scaled to 100 mm/hr (by 100/92) and that the 12 mm/hr can be scaled to 15 mm/hr (by 15/12). With this scale factor incorporated and assuming the same distribution curve shapes (Marshall-Palmer distributions), the calculated RSL can be directly compared with measured rainfall spectrum levels.

The first comparison, 92 mm/hr (100 mm/hr), is shown in Figure 35. The calculated RSL, using only Type II drops, is within about 5 dB of the measured (OTP) RSL from 7 - 20 kHz. The two differ by approximately 10 dB for frequencies less than 7 kHz, but the *slopes* are equal. This could be due to a different DSD for the calculated and measured rainfall. Above 13 kHz, some of the difference will be made up by Type I drops, which radiate sound at approximately 15 kHz. The results, however, are very promising. The "low confidence" markers in Figure 35 indicate a region in which the

OTP hydrophone calibration is in question. An in-place calibration of the OTP hydrophone is currently being conducted to correct this.
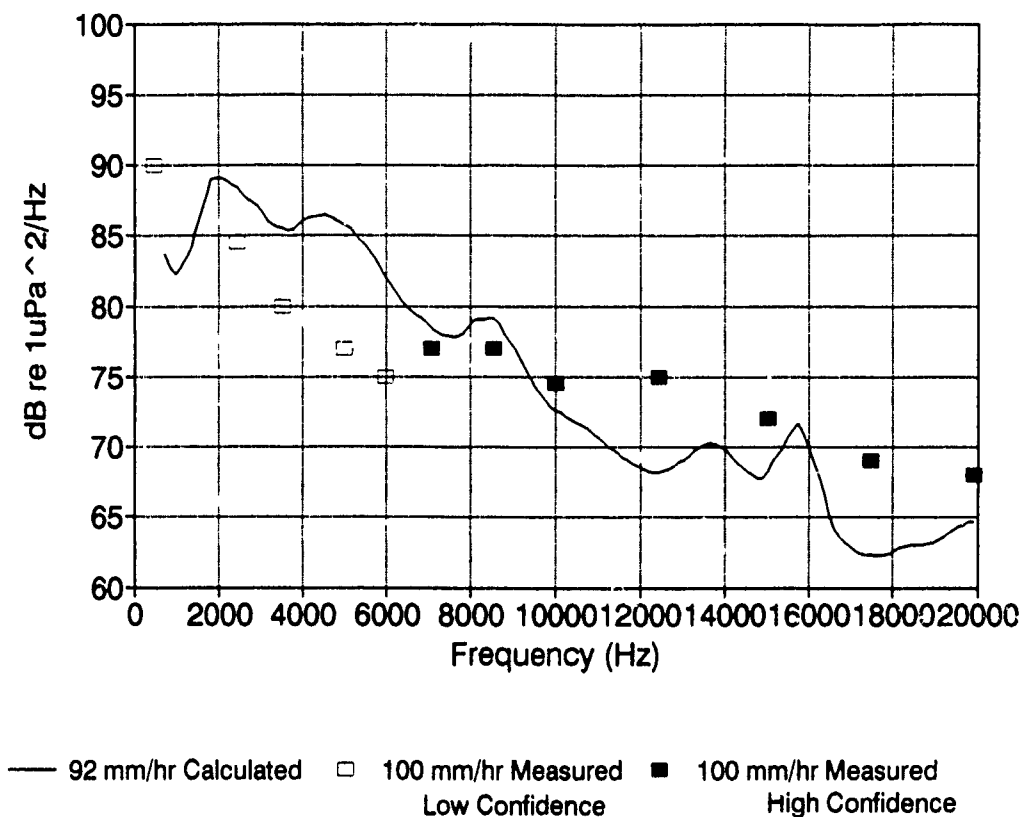


**Figure 35.    100 mm/hr Rainfall Rate: Calculated vs. Measured at OTP**

The second comparison, 12 mm/hr (15 mm/hr), is shown in Figure 36. The calculated RSL is within 3 dB for most of the frequency range of interest and within 5 dB over the entire range and again using only Type II drops. This shows *very* good agreement between the calculated and measured (OTP) rainfall spectrum levels and again confirms the theory that the sound radiation researched in this work can be used to predict the underwater spectrum of natural rainfall.
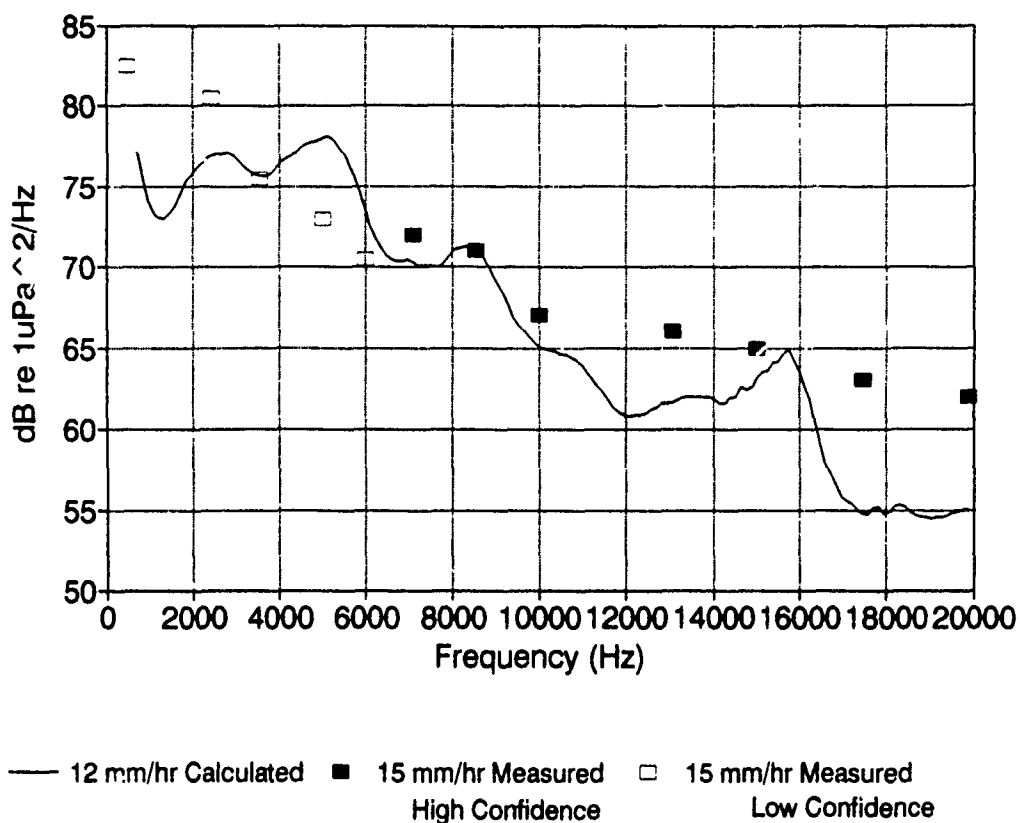
**Figure 36.** 15 mm/hr Rainfall Rate: Calculated vs. Measured at OTP

The temperatures of the raindrops and of the ocean water were not known in the field work used for these two comparisons. It is assumed that the rain had been falling for a sufficient length of time to equalize the drop and surface temperatures. The calculated results are based on a 0 °C temperature difference between the drop and surface temperatures and 35 ppt salinity (for the comparisons with the OTP measured data). If the *actual* field parameters were different than those assumed, the results will be affected as described in the next two chapters.

# VII. DEPENDENCE OF SOUND RADIATION ON TEMPERATURE

## A. BACKGROUND

The previous results assume that the sound radiated from the raindrops is independent of the parameters describing the ocean such as temperature, salinity, surface tension, surface spectrum, etc. Any additional factor leads to a more complicated calculation of the RSL. The next step is to evaluate each of these parameters to determine if the sound radiated by large raindrops is affected, and then to quantitatively evaluate the effect. Temperature is the easiest parameter to change, and since the 4.2 mm diameter drop produces the highest percentage of bubbles, it is the best drop diameter with which to begin.

## B. RESULTS FOR 4.2 MM DIAMETER DROPS

Initially, it was thought that a change in the surface temperature of the water would affect the sound radiated, most likely because of the change in density (acoustic impedance) and viscosity of the surface water. The results of this experiment, changing surface temperature, led to seemingly erratic results. A change in the total radiated energy was evident, but it could not be directly correlated to the change in surface temperature (two examples are shown in Figure 37 and Figure 38). Each curve is the average of 50 drops. However, a closer examination of the records for the experiment showed that the *drop* temperature had also varied from day to day.
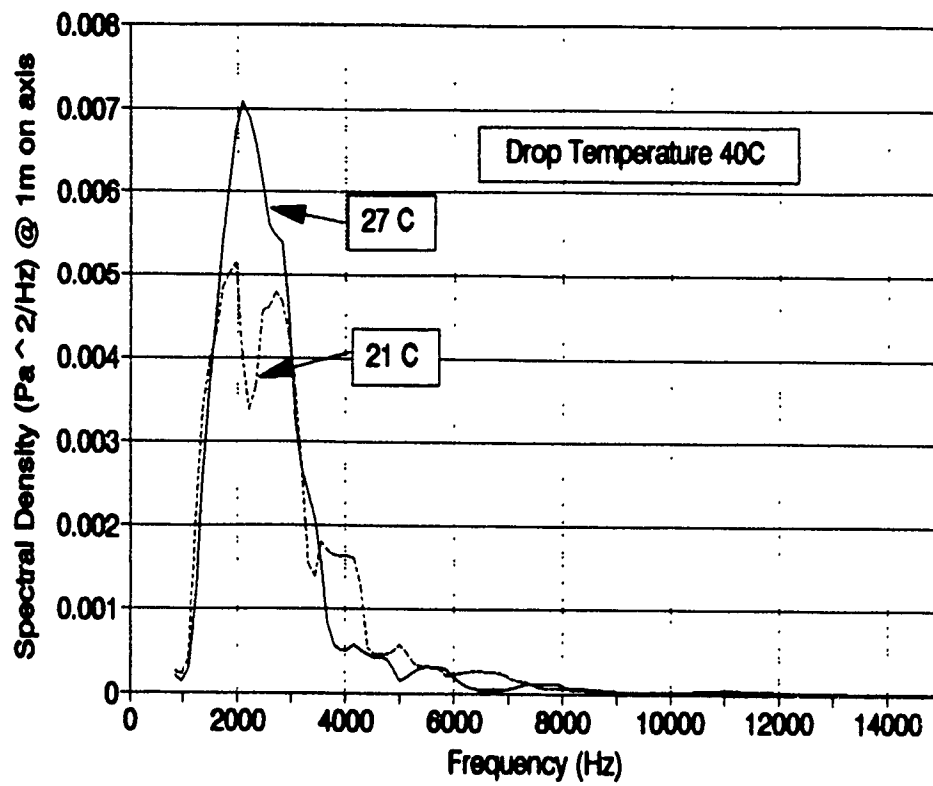
Figure 37.    Dependence of Sound Radiation on Change in Surface Temp.
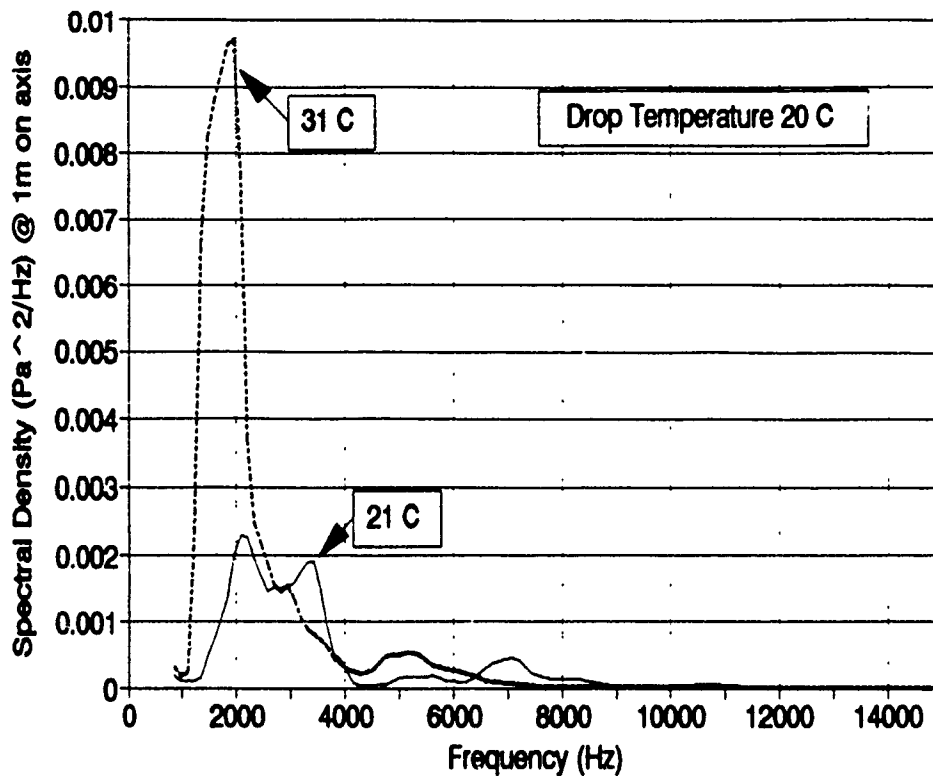
**Figure 38.** Dependence of Sound Radiation on Change in Surface Temp.

The next step was to conduct a similar set of experiments, this time varying the *drop* temperature. Again, the results were seemingly erratic as there was no direct correlation between drop temperature and the total energy radiated (Figure 39). Each curve is the average of 50 drops. Again, an examination of the records for the experiment showed that the surface temperature had varied slightly for each experiment.
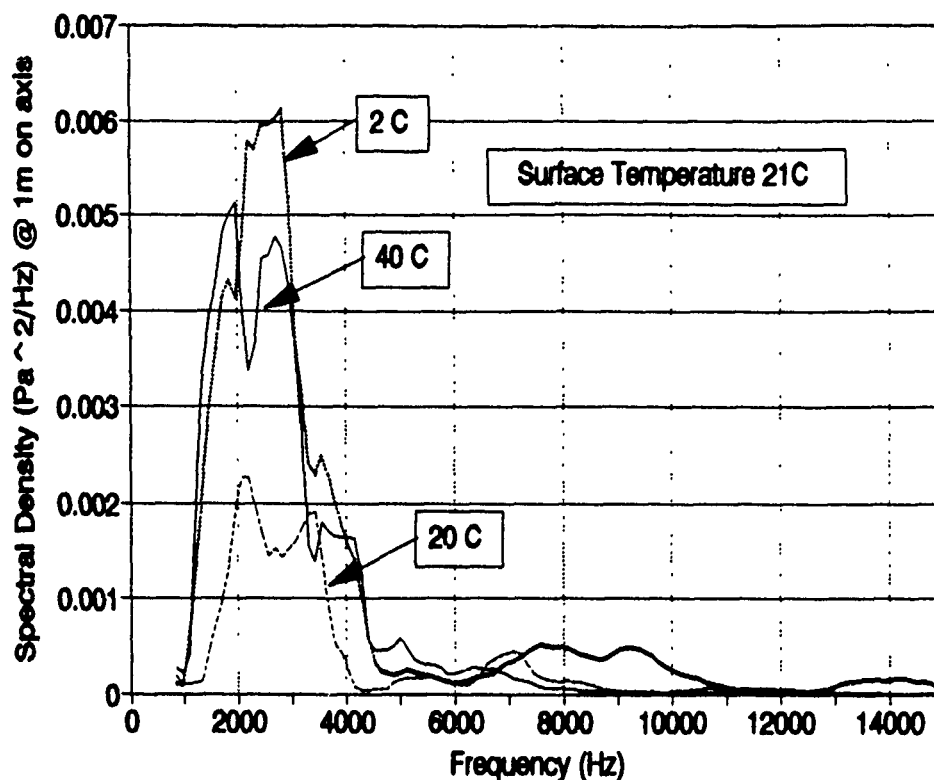
**Figure 39.** Dependence of Sound Radiation on Change in Drop Temperature

The next logical step was to compare the change in energy radiated with the *difference* between the drop temperature and surface temperature. The result was a direct, linear correlation between the energy radiated and the absolute difference in temperature between drop and surface. The resultant values are plotted in Figure 40 with a linear regression fit to the energy radiated. The total energy radiated from an *average* 4.2 mm diameter raindrop is given by:

$$\text{Energy} = 540 + 38 \, |T_s - T_d| \tag{19}$$

where Energy is in pJ, $T_s$ is the surface temperature and $T_d$ is the drop temperature in degrees centigrade. This equation is accurate to within 15 % of the measured total energy over the range of temperature difference expected in normal rainfall ( < 15 C) and is based on the results from 300 drops.
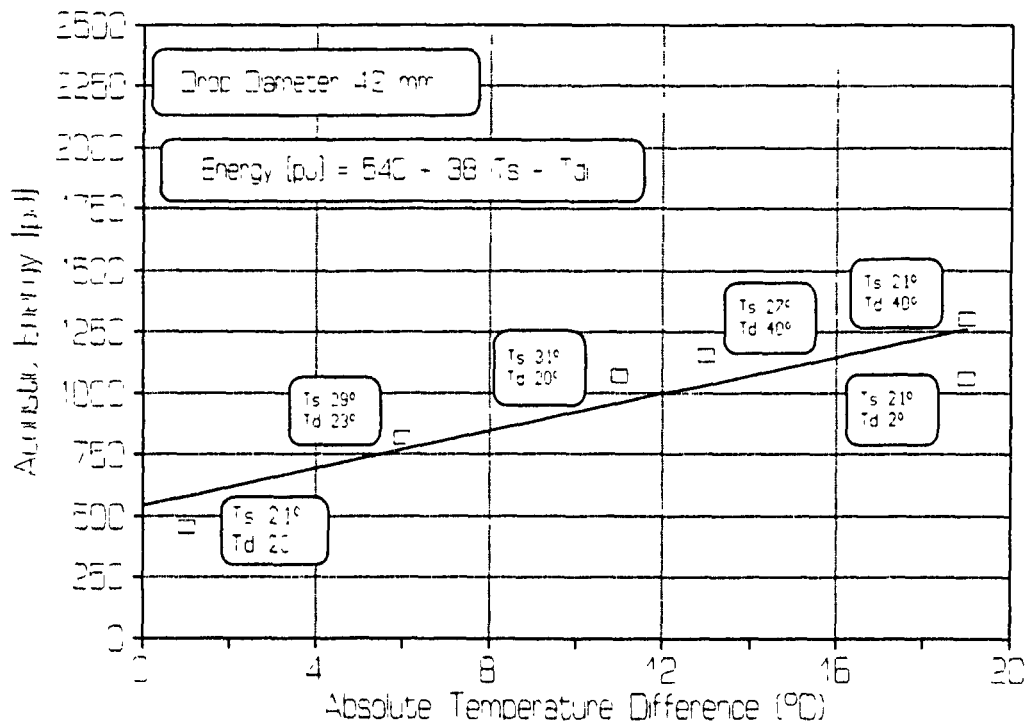
Figure 40.  Total Energy of 4.2 mm Drop vs Drop/Surface Temperature Difference

For comparison with the energy radiated from other drop sizes, as given in Chapter V, the energy radiated by each set of drop/surface temperature combination is tabulated below in Table 11.

## C.  RESULTS FROM ADDITIONAL DROP DIAMETERS

To verify the theory that radiated sound energy increases with the difference in drop/surface temperature, a total of approximately 250 drops were taken in three additional drop sizes (3.6 mm, 4.0 mm and 4.6 mm). Radiated energy in pJ is given by:

$$\text{3.6 mm } (25\mu l) \quad \text{Energy} = 172 + 20 \ |T_s - T_d| \tag{20}$$

$$\text{4.0 mm } (32.5\mu l) \quad \text{Energy} = 308 + 25 \ |T_s - T_d| \tag{21}$$

$$\text{4.2 mm } (40\mu l) \quad \text{Energy} = 540 + 38 \ |T_s - T_d| \tag{22}$$

$$\text{4.6 mm } (50\mu l) \quad \text{Energy} = 555 + 49 \ |T_s - T_d| \tag{23}$$

### Table 11. ENERGY RADIATION OF 4.2 MM DROP: DEPENDENCE ON TEMPERATURE DIFFERENCE

| Surface Temperature (C) | Drop Temperature (C) | Temperature Difference (C) | Energy Radiated (pJ) |
|---|---|---|---|
| 21 | 20 | 1 | 450 |
| 29 | 23 | 6 | 820 |
| 31 | 20 | 11 | 1100 |
| 27 | 40 | -13 | 1200 |
| 21 | 40 | -19 | 1100 |
| 21 | 2 | 19 | 1300 |

## D. NORMALIZED TEMPERATURE DEPENDENCE

It is possible that the increase in energy which is seen for different drop sizes as the difference between drop temperature and surface temperature increases may be due to mixing and energy exchange which takes place on the edge of the crater and the turbulent jet. It is therefore reasonable to postulate that the excess sound energy radiated when there is a temperature difference is also proportional to the excess drop volume beyond the minimum volume (7 $\mu$l = 2.2 mm diameter) for which Type II bubbles are created. The sound energy is then normalized by dividing the average energy per drop by excess drop volume (drop volume - 7 $\mu$l).

The result of volume normalization is shown in Figure 41. which shows a strong correlation between temperature difference and the sound energy radiated for drop volumes between 10 $\mu$l (2.7 mm) - 50 $\mu$l (4.6 mm) given by:

$$\text{Energy}_{II} = (12.4 + 1.03\,\Delta T) \times (\text{Volume} - 7) \qquad (24)$$

where energy is in pJ, $\Delta T$ is in degrees centigrade and volume is in $\mu$l.

Drops less than 10 $\mu$l have significant contributions from the impact due to the small fraction of bubbles produced. Since the impact radiated energy does not appear to be affected by temperature differences, drops less than 10 $\mu$l will most likely not show the same dependence of radiated energy on temperature.
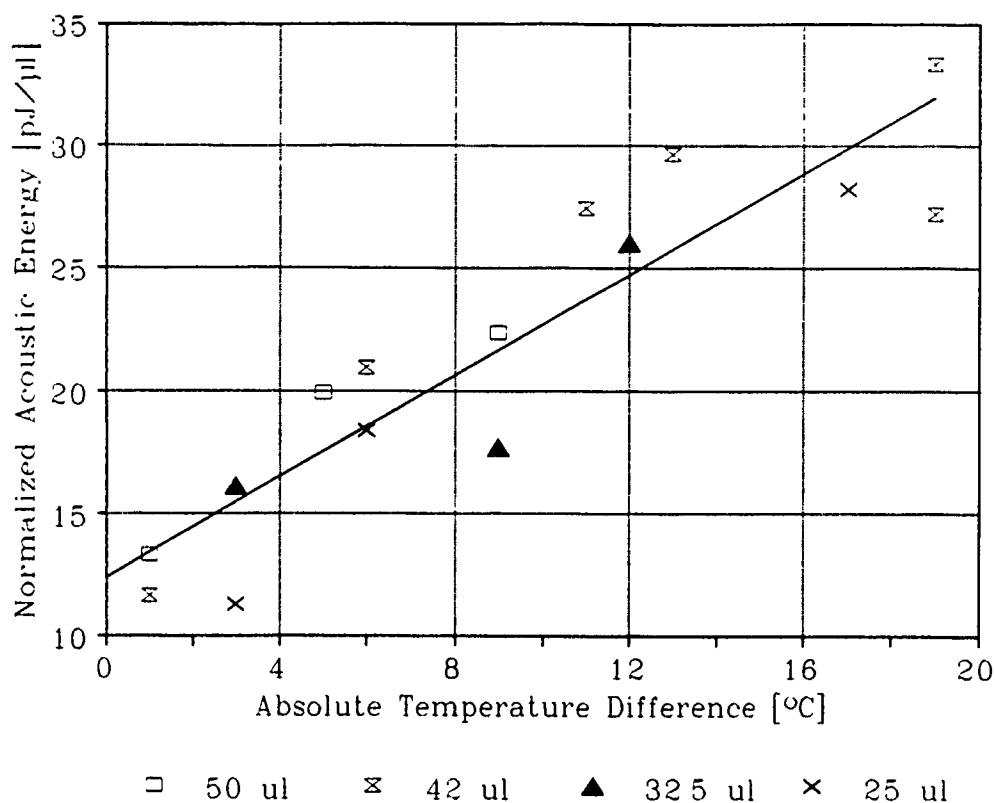
**Figure 41.** Dependence of Normalized Sound Energy on Drop Volume and Temperature Difference - Fresh Water

## E. TEMPERATURE DEPENDENCE SUMMARY

Temperature has been shown to cause a predictable variation in the sound radiated by raindrops of diameters 2.2 mm to 4.6 mm. The radiated energy depends on the absolute difference between drop temperature and surface temperature.

This effect may explain the abnormally high sound levels at the beginning of a storm compared to later in the same storm (McGlothin, 1991). When a storm begins, the drop and surface temperatures are most likely different. As the storm continues, mixing at the surface will minimize the temperature difference and a lower radiated energy will result, even for an identical drop size distribution. Other explanations for the decrease in sound levels have been offered, such as growing numbers of bubbles from the rainfall forming a bubble-filled layer which causes increased attenuation between the surface source and the underwater hydrophone. The bubble layer explanation, however, is speculative and has not been experimentally measured.

# VIII. DEPENDENCE OF SOUND RADIATION ON SALINITY

## A. BACKGROUND

Salinity, like temperature, causes a change in the density, surface tension and viscosity of water. In this experiment, the change will be the most drastic: fresh water to salt water. Unlike the case of temperature, which changes radically over even small areas of the ocean surface, salinity is fairly constant (within 10%) over the world's oceans. Zero salinity is the case for lakes and estuaries. The effect that it has on sound radiation should therefore be uniform over any ocean or lake considered.

## B. RESULTS

Approximately 100 pounds of "sea salt" was added into the redwood tank, yielding synthetic sea water with a salinity of 34.6 ±0.05 ppt. Over 110 additional fresh water drops in four drop diameters were studied to investigate the effects of saline surface water.

In all drop diameters, the sound energy radiated in saline water was *substantially less* than in fresh water. However, the *shape* of the spectrum remains unchanged compared to the fresh water case (i.e., dominant bubble frequency, secondary bubble, etc.) The summary in Table 12 shows an average of *45%* less energy radiated into saline water as compared to fresh water. Therefore, the rainfall spectrum level from identical rainfalls over fresh and salt water will differ by approximately 3 dB.

Table 12. SALINITY EFFECT SUMMARY.

| Drop Diameter [mm] | Volume [μl] | Energy, Salt Water [pJ] | Energy, Fresh Water [pJ] | Salt/Fresh Ratio |
|---|---|---|---|---|
| 3.6 | 26 | 136 | 293 | 47% |
| 4.0 | 32.5 | 221 | 458 | 48% |
| 4.2 | 42 | 271 | 683 | 40% |
| 4.6 | 50 | 353 | 847 | 42% |

Futher experiments conducted by LT Chris Scofield using intermediate salinity values have shown a linear relation between the energy radiated and the surface water salinity. The energy radiated by Type II drops can therefore be described by:

$$\text{Energy}_{II} = (12.4 + 1.03\Delta T) \times (\text{Volume} - 7) \times (1 - \frac{\text{Salinity}}{77}) \qquad (25)$$

where energy is in pJ, $\Delta T$ is in degrees centigrade, volume is in $\mu$l and salinity is in ppt.

# IX. CONCLUSION

Not only has the original goal of quantifying the effects of ocean parameters on the sound radiation of large terminal velocity raindrops been met, but answers have been provided for other phenomena as well. This work has shown that:

- There is a quantifiable relationship between drop diameter (2.7 mm - 4.6 mm) and the frequency of the peak spectral density ranging from 8.5 kHz to 1.8 kHz respectively.

- There is a quantifiable relationship between drop diameter and the average sound energy radiated by impacts.

- The percentage of large bubbles created by drops of diameter 2.2 mm to 4.8 mm is statistically predictable and ranges between 0 % at 2.2 mm to 62% at 3.7 mm.

- Additional sources of sound radiation (wobble and secondary bubble) have been identified and their secondary contribution to the overall rainfall spectrum has been quantified.

- The average energy per raindrop has been quantified for drop diameters between 2.7 mm - 4.6 mm and its dependence on volume, temperature and salinity has been shown.

- Spectrum levels due to rainfall can be calculated for measured drop size distributions, and they compared favorably with sound from similar rainfall rates measured at sea.

- Radiated energy is directly proportional to the absolute difference between surface temperature and drop temperature. A threefold increase in radiated energy occurs when the temperature difference increases from 0 °C to 19 °C.

- Radiated energy depends strongly on the salinity of the surface water. Sound energy radiation is 45% less in saline water as compared to fresh water.

- An empirical relation valid for drops of diameter 2.7 mm to 4.6 mm has been developed relating the average sound energy radiated per raindrop to volume, drop/surface temperature difference and salinity:

$$\text{Energy}_{\text{II}} = (12.4 + 1.03\Delta T) \times (\text{Volume} - 7) \times \left(1 - \frac{\text{Salinity}}{77}\right)$$

where energy is in pJ, $\Delta T$ is in °C, volume is in $\mu$l and salinity is in ppt.

The problem of calculating a rainfall spectrum level for a given drop size distribution has been essentially solved in terms of volume, temperature and salinity effects. The inverse problem, obtaining the drop size distribution for a given rainfall spectrum level, is much more complicated, but it can be solved given the results of this work. Since the corresponding total rainfall rate can be determined from this calculated drop size dis-

tribution, the question of how to determine both total rainfall rate and drop size distribution by remote sensing is well on its way to being answered.

# REFERENCES

1. Wenz, G.W., "Acoustic ambient noise in the ocean: spectra and sources," *J. Acoust. Soc. Am.* 34, 1936-1956 (1962)

2. Lemon, D.D. and Farmer, D. M., "The influence of bubbles on ambient noise in the ocean at high wind speeds," *J. Phys. Ocean.* 14, 1762-1778 (1984).

3. Scrimger, J.A., Evans, D.J. and Yee, W., "Underwater noise due to rain - open ocean measurements," *J. Acoust. Soc. Am.* 85, 726-731 (1989).

4. Tan, C., "A characterizaton of underwater sound produced by heavy precipitation," Master's Thesis, Naval Postgraduate School, Monterey, CA 93943 (1989)

5. Franz, G., "Splashes as sources of sounds in liquids," *J. Acoust. Soc. Am.* 31, 1080 - 1096 (1959)

6. Minnaert, M., "On musical air-bubbles and the sounds of running water," *Phil. Mag.* 16, 235-248 (1933)

7. Kurgan, A., "Underwater sound radiated by impacts and bubbles created by raindrops," Master's Thesis, Naval Postgraduate School, Monterey, CA, 93943 (1989)

8. Pumphrey, H.C., Crum, L.A., and Bjorno, L., "Underwater sound produced by individual drop impacts and rainfall," *J. Acoust. Soc. Am.* 85, 1518-1526 (1989)

9. Medwin, H., Kurgan, A., and Nystuen, J.A., "Impact and bubble sound from raindrops at normal and oblique incidences," *J. Acoust. Soc. Am.* 88(1), 413-418 (1990)

10. Nystuen, J.A. and Farmer, D.M., "Precipitation in the Canadian Atlantic storms program: Measurements of the acoustic signatures," *Atmosphere-Ocean* 27, 237-257 (1989)

11. Nystuen, J.A., "An explanation of the sound generated by light rain in the presence of wind," to appear in *Natural Physical Sources of Underwater Sound*, ed. B.R. Kerman, Kluwer Academic Press (1991)

12. Snyder, D.E., "Characteristics of sound radiation from large raindrops," Master's Thesis, Naval Postgraduate School, Monterey, CA 93943 (1990)

13. Medwin, H. and Beaky, M.M., "Bubble sources of the Knudsen sea noise spectra," *J. Acoust. Soc. Am.* 86, 1124-1130 (1989)

14. Nystuen, J.A. and Farmer, D. M., "The influence of wind on the underwater sound generated by light rain," *J. Acoust. Soc. Am.* 270, 270-274 (1987)

15. Oguz, H.N. and Prosperetti, A., "Bubble entrainment by the impact of drops on liquid surfaces," *J. Fluid Mechanics* 218, 143-162 (1990)

16. Longuet-Higgins, M.S., "An analytical model of sound production by raindrops," *J. Fluid Mechanics* 214, 395-410 (1990)

17. Pruppacher, H.R. and Pitter, R.L., "A semi-emperical determination of the shape of cloud and rain drops," *J. Atmos. Sci.* **28** 86-94 (1971)

18. Pumphrey, H.C. and Crum, L.A., "Sources of ambient noise in the ocean: An experimental investigation," Technical Report, National Center for Physical Acoustics (1989)

19. Pumphrey, H.C., "Underwater rain noise - the initial impact component," Proceedings of the U.K. Institute of Acoustics, May 1991

20. Pumphrey, H.C. and Elmore, P.A., "The entrainment of bubbles by drop impacts," *J. Fluid Mechanics* **220**, 539-567 (1990)

21. Devin, C., "Damping of pulsating air bubbles in water," *J. Acoust. Soc. Am.* **31**, 1654 (1959)

22. Scrimger, J.A., Evans, D.J., McBean, G.A., Farmer, D.M., and Kerman, B.R., "Underwater noise due to rain, hail and snow," *J. Acoust. Soc. Am.* **81**, 79-86 (1987)

23. McGlothin, C., "Ambient sound in the ocean induced by heavy precipitation and the subsequent predictability of rainfall rate," Master's Thesis. Naval Postgraduate School, Monterey, CA 93943 (1991)

24. Marshall, J.S. and Palmer, W. McK., "The distribution of raindrops with size," *J. Meteor.* **5**, 165-166 (1948)

# INITIAL DISTRIBUTION LIST

No. Copies

1. Defense Technical Information Center    2
   Cameron Station
   Alexandria, VA  22304-6145

2. Library, Code 52    2
   Naval Postgraduate School
   Monterey, CA  93943-5002

3. Department of Physics    5
   Attn: Professor H. Medwin, Code PH/Md
   Naval Postgraduate School
   Monterey, CA 93943-5002

4. Department of Physics    1
   Attn: Professor A. A. Atchley, Code PH/Ay
   Naval Postgraduate School
   Monterey, CA 93943

5. Department of Oceanography    1
   Attn: Professor J. A. Nystuen, Code OC/Ny
   Naval Postgraduate School
   Monterey, CA  93943

6. Dr. Marshall Orr    1
   Office of Naval Research (Code 11250A)
   800 N. Quincy Street
   Arlington, VA  22217

7. Dr. John R. Proni    1
   NOAA/AOML/OAD
   4301 Rickenbacker Causeway
   Miami, FL 33149

8. LT Peter W. Jacobus    1
   c/o Dorothy Crain
   116 Second St.  Apt. 6
   Pacific Grove, CA 93950

9. LT Chris Scofield    1
   Weapons Engineering Department UX03
   Naval Postgraduate School
   Monterey, CA  93943